

National University Of Ho Chi Minh City
University Of Science
Faculty Of Physics- Engineering Physics

Vo Chau Duc Phuong

**Calculation of the Linear-Absorption Spectrum of
an Ideal Two-Dimensional System of MoS₂**

Graduation Bachelor Thesis
Merits Program

Ho Chi Minh city, July-2024

Commitment

I commit to independently conducting the calculation of the linear-absorption spectrum of an ideal two-dimensional system of MoS₂ for my bachelor thesis, under the supervision of Dr. Huynh Thanh Duc, and with guidance from Master Le Minh Chau.

Acknowledgments

Mục lục

1	Introduction	6
1.1	Overview of Two Dimensional Material Research	6
1.2	Methods and Results	6
1.3	Overview on Theories	7
2	Theories	8
2.1	Tight-Binding Theories	8
2.2	Three Band Tight-Binding Model	9
2.3	System Hamiltonian	12
2.3.1	First Quantization Hamiltonian	12
2.3.2	Second Quantization Hamiltonian	13
2.4	Semiconductor Bloch Equation	14
2.5	Polarization Density	15
3	Numerical Methods	16
3.1	Numerical Sum Over k-Space	16
3.2	Cut Off K-point Technique	17
3.3	Numerical Analyzing	18
4	Results and Discussion	19
5	Conclusion and Further	22
	Appendices	23
A	Electromagnetic Field - Charge Interaction Hamiltonian	23
B	Electron - Electron Interaction Hamiltonian	24
C	Motion Equation	26
D	Dipole Matrix Elements	28

Danh sách hình vẽ

1	TMD structure and its first Brillouin zone	9
2	Band structure of MoS ₂ material along $M \rightarrow -K \rightarrow \Gamma \rightarrow K \rightarrow M$ direction	11
3	Rhombus primitive unit cell in compare with hexagon primitive unit cell (the first Brillouin zone)	16
4	New Basics Based on the rhombus unit vectors	17
5	k-radius show the cutoff circle around K' points	17
6	Electric field on Ox direction and it Fourier Transform	18
7	Measured absorption spectrum of MoS ₂	19
8	Absorption Spectrum with difference T_2	20
9	Absorption Spectrum with difference dielectric ε and without Coulomb interaction . .	21
10	Absorption Spectrum with difference number of k-points	22

Danh sách bảng

1	Fitting parameters in three-band tight-binding model for MoS_2	11
2	Exciton binding energy with difference dielectric	20

Thesis Information

Name of Thesis: Calculation of the Linear-Absorption Spectrum of MoS₂

Major: Theoretical Physics

Student's name: Vo Chau Duc Phuong

Year: 2020-2024

Supervisor: Dr. Huynh Thanh Duc

Department: Theoretical of Physics

Faculty: Physics - Engineering Physics

At: VNUHCM - University of Science

Abstract

Transition Metal Dichalcogenides (TMD) are promising semiconductors due to their extraordinary electronic and optoelectronic properties. Before calculating the nonlinear optical properties of this material, we need to calculate the linear absorption spectrum. In monolayer TMD, the Coulomb interaction heavily influences the increase in exciton binding energies. Therefore, the independent electron approximation model is not reliable for simulating the experiment, especially in low-dimensional systems. In this work, we use a minimum three-band Tight-Binding Hamiltonian for the band structure calculation and the Semiconductor Bloch Equation to model the response of electron density in MoS₂ material to a laser over time to calculate the Linear Absorption Spectra (LAS) and extract the Exciton binding energy from it.

Novelty Of Thesis

Our calculation on exciton binding energy (0.25 eV) based on this model proves to agree with the experiment and proves to be more accurate than some previous theoretical, which predict exciton binding energy too large (0.5-1 eV).

Applications/ Applicability/ Perspective

From this work, we can use it to calculate other effects which affected by Exciton binding energy such as photo-current, high harmonic generation, and high-order sideband generation. Increase the density of the k-point for better convergence results. Take into account the shield coulomb interaction when increasing the density of electrons on the conduction bands when excess of the low excitation limit for full absorption spectra.

1 Introduction

1.1 Overview of Two Dimensional Material Research

The researcher has dedicated many years to studying Graphene, with hopes that it could potentially serve as the new silicon, enabling the continuation of Moore’s law on the CPU chip dice. However, in recent years, the number of papers on Graphene properties has reached thousands yearly, indicating that research on ‘simple graphene’ has peaked.¹ Therefore, the researchers shifted their focus from working solely with Graphene to exploring applications and other two-dimensional materials.

Atomically thin two-dimensional (2D) forms of layered transition metal dichalcogenides (TMD) have recently gained significant scientific and technological interest since the first five years of the Graphene boom.^{1;2} TMD has the chemical composition MX_2 , so it has a wide range of materials. They include both metals and semiconductors, for example NbS₂, NbSe₂, TaS₂, TaSe₂, β -MoT₂ and Td-WTe₂ are bulk metals while the ReS₂, ZrS₂, MoS₂, WS₂, MoSe₂, WSe₂ and α -MoTe₂ are semiconductors. The structure of TMD consists of multiple monolayers bonded by van der Waals forces, with in-plane stability ensured by strong covalent bonds. Among various transition metal dichalcogenides, the group-VIB (M = Mo, W; X = S, Se) is stable in both mono- and few-layers in the air at room temperature.¹ These two-dimensional semiconductors have a direct band gap in the visible frequency range, stable and excellent mobility at room temperature^{2;3} and promise to become a good candidate for electronic and optoelectronic applications. Its nanotube structure has been researched and shows its potential to become the new solar cell material^{3–6}.

Transition metal dichalcogenides (TMD) exhibit non-centrosymmetry in monolayers form, resulting in unique properties in electronic, spintronics, optoelectronics, superconduction, and valleytronic applications^{7;8}. Additionally, significant Spin-Orbit Coupling in TMD creates a considerable split in the band structure valley. The low dimension system causes the reduced screening of Coulomb interaction outside the monolayer’s plane, resulting in large exciton binding energies^{9;10}. These binding energies are notably higher than those observed in typical III-V materials, implying that many-body interactions play a key role in determining the electronic and optical properties of these materials. In some previous work, only the nearly free electron approximation has been taken into account and did not give good accuracy on the results as the key role of many-body interactions in the system. Furthermore, previous theoretical works have predicted the binding energy too large^{11–14} when compared with experiment¹⁰ and other more accurate theoretical works^{9;10}.

1.2 Methods and Results

In our current research, our main objective is to identify the appropriate model for estimating the exciton binding energy while aligning with experimental data. The key challenge is to identify a model that strikes a balance between simplicity and accuracy. Our primary focuses on investigating the properties of transition metal dichalcogenides (TMD). Several models, such as ab initio calculations^{9;11–14} and parabola approximation^{15;16}, have been developed and employed to simulate the band structure. It is important to note that these models have limitations as they can only calculate around highly symmetric points and not across the entire Brillouin zone (BZ). In our study, we are using a three-band tight-binding model to calculate properties across the entire BZ, which should give us results that better match experimental data.

From now and for later in this work, we use the minimal three-band tight-binding Hamiltonian¹⁷ to calculate the band structure by determining the eigenvalues at each k-point. The momentum matrix for the velocity gauge matrix will be calculated using finite differentiation, and then utilized to compute the dipole matrix. We plan to solve the Semiconductor Bloch Equations (SBE) using the

RungeKutta 4th order method to numerically find the time-independent density evolution. Based on this density, we can derive the polarization, current density, and other measurable physical parameters. After obtaining the polarization, we will perform a Fourier transform to obtain the absorption spectrum.

In our analysis, we concentrated on the low excitation regime to examine the linear absorption spectra. We were able to concentrate on scenarios where the electron density in the conduction bands is significantly lower than that in the valence bands. The results showed a significant exciton binding energy, which closely matched both experimental measurements and theoretical expectations. These discoveries allow us to predict the existence of smaller excitons and use the binding energy to investigate other effects influenced by the Coulomb interaction. We were able to concentrate on scenarios where the electron density in the conduction bands is significantly lower than that in the valence bands. The results showed a significant exciton binding energy, which closely matched both experimental measurements and theoretical expectations. These discoveries allow us to predict the existence of smaller excitons and use the binding energy to investigate other effects influenced by the Coulomb interaction.

1.3 Overview on Theories

The theoretical part includes the following topics:

- Theory on the Tight-Binding Approximation: Starting from the Schrödinger equation for the independent charge approximation with the LCAO ansatz. Show the on-site and hopping energies, as well as the overlap densities parameters for the semi-empirical formalism.
- Derivation of light-matter interaction for charge systems, using the velocity gauge.
- Derivation of Semiconductor Bloch Equation in the Hartree-Fock approximation (HFA), along with the dephasing T_2 approximation.
- Steps to numerically calculate the polarization density and linear absorption spectrum.

2 Theories

2.1 Tight-Binding Theories

We start from Hamiltonian H for many-body system in the independent electron approximation:

$$H = \sum_{\lambda} H^{1e}(\mathbf{r}_{\lambda}). \quad (1)$$

In the independent electron approximation, the stationary state of an electron in a solid is presented by the one-particle time-independent Schrödinger equation:

$$H_{1e}\psi_{\lambda\mathbf{k}}(\mathbf{r}) = \left(-\frac{\hbar^2\nabla^2}{2m} + V_0(\mathbf{r}) \right) \psi_{\lambda\mathbf{k}}(\mathbf{r}) = \varepsilon_{\lambda}(\mathbf{k})\psi_{\lambda\mathbf{k}}(\mathbf{r}). \quad (2)$$

We assume that the electrons stay close to the atomic sites and that the electronic wave functions centered around neighboring sites have little overlap. There is almost no overlap between wave functions for electrons that are separated by two or more atoms. Therefore, the wave function of an electron will have the similar form of atomic orbital and we can describe it in the form of Linear Combination of Atomic Orbitals (LCAO):

$$\psi(\mathbf{r}) = \sum_{n=1}^N \sum_{c=1}^{N_c} \sum_{\alpha=1}^{N_{orb}} c_{\alpha c}(\mathbf{R}_n) \phi_{\alpha}(\mathbf{r} - \mathbf{R}_n - \mathbf{r}_c). \quad (3)$$

In which ϕ_{α} is orbital wave function of an atomic, \mathbf{R}_n is position of Bravais unit cell, \mathbf{r}_c is relative position of the atom in that cell, N_{orb} is number of orbital of an atom, N_c is number of atom in an unit cell and N is the number of unit cell in the lattice. Based on LCAO wave function, we can construct the Bloch wave function in the following form:

$$\psi_{\mathbf{k}}(\mathbf{r}) = \sum_{c=1}^{N_c} \sum_{\alpha=1}^{N_{orb}} C_{\alpha c}(\mathbf{k}) \sum_{n=1}^N e^{i\mathbf{k}(\mathbf{R}_n + \mathbf{r}_c)} \phi_{\alpha}(\mathbf{r} - \mathbf{R}_n - \mathbf{r}_c) \quad (4)$$

This wave function satisfies the Bloch theorem. Include (4) in the one-particle time-dependent Schrödinger equation (2), multiply with $e^{i\mathbf{k}\mathbf{r}'} \phi_{\alpha'}^*(\mathbf{r} - \mathbf{r}_c')$ on the left, and take the integral over \mathbf{r} to have:

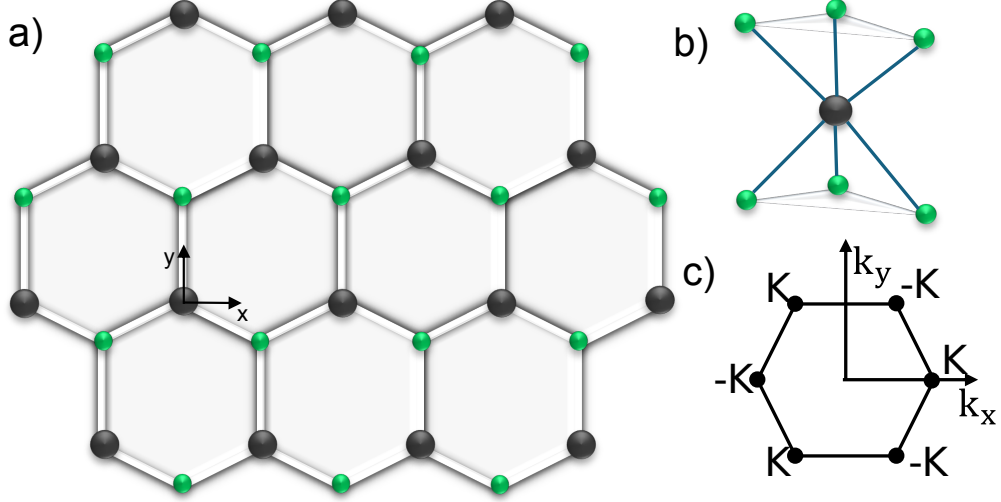
$$\sum_{c=1}^{N_c} \sum_{\alpha=1}^{N_{orb}} (H_{\alpha'c',\alpha c}(\mathbf{k}) - \varepsilon(\mathbf{k}) S_{\alpha'c',\alpha c}(\mathbf{k})) C_{\alpha c}(\mathbf{k}) = 0. \quad (5)$$

In which on-site hopping energies $H_{\alpha'c',\alpha c}(\mathbf{k})$ and overlap density $S_{\alpha'c',\alpha c}(\mathbf{k})$ defined by:

$$H_{\alpha'c',\alpha c}(\mathbf{k}) = \sum_{n=1}^N e^{i\mathbf{k}(\mathbf{R}_n + \mathbf{r}_c - \mathbf{r}_{c'})} \int d\mathbf{r} \phi_{\alpha'}^*(\mathbf{r} - \mathbf{r}_{c'}) H_{1e} \phi_{\alpha}(\mathbf{r} - \mathbf{R}_n - \mathbf{r}_c), \quad (6)$$

$$S_{\alpha'c',\alpha c}(\mathbf{k}) = \sum_{n=1}^N e^{i\mathbf{k}(\mathbf{R}_n + \mathbf{r}_c - \mathbf{r}_{c'})} \int d\mathbf{r} \phi_{\alpha'}^*(\mathbf{r} - \mathbf{r}_{c'}) \phi_{\alpha}(\mathbf{r} - \mathbf{R}_n - \mathbf{r}_c). \quad (7)$$

Solving the eq. (5) in several k -point, we will have the wave functions and energy. In the semi-empirical formalism, these integrals shall be left as phenomenological parameters. By finding the eigenvalues of this Hamiltonian at every k -point, we can construct the band structure for the system.



Hình 1: (a) Top view of monolayer MX_2 . The large sphere is \mathbf{M} and the small sphere is \mathbf{X} . (b) sideview of monolayer MX_2 . (c) The 2D first Brillouin zone with special \mathbf{k} points.

2.2 Three Band Tight-Binding Model

In previous ab initio calculations^{18–22}, Prof. Xiao and his colleague discovered that the monolayer of MX_2 with D_{3h} point-group symmetry has a structure as shown in Figure 1. They found that the Bloch states of the monolayer MoS_2 near the band edges are primarily composed of $Mo-d$ orbitals, particularly the d_{z^2} , d_{xy} , and $d_{x^2-y^2}$ orbitals. To accurately capture the band-edge properties in the K and K' valleys, they developed an approximate model for group VII-B TMD consisting of only these three bands and neglecting $X-p$ orbitals, and then extended it to fit the entire Brillouin Zone¹⁷. Denote three M-d bands as:

$$|\phi_1\rangle = d_{z^2}, \quad |\phi_2\rangle = d_{xy}, \quad |\phi_3\rangle = d_{x^2-y^2}. \quad (8)$$

As discussed above, the Bloch states near the band edges mostly consist of Mo-d orbital, therefore we ignore the \mathbf{r}_c and the sum over it in hopping energy (6). Each pair of difference bases is assumed to be orthogonal; therefore the overlapping matrix element become:

$$S_{\alpha,\alpha'}(\mathbf{k}) = \delta_{\alpha\alpha'}.$$

The hopping energies eq.(6) between the atomic orbitals $|\phi_\mu\rangle$ at 0 and $|\phi_{\mu'}\rangle$ at lattice vector \mathbf{R} can be obtained as:

$$H_{\mu\mu'}(\mathbf{k}) = \sum_{\mathbf{R}} e^{i\mathbf{k}\cdot\mathbf{R}} \langle \phi_\mu(\mathbf{r}) | \hat{H} | \phi_{\mu'}(\mathbf{r} - \mathbf{R}) \rangle.$$

Confined by the symmetry of the system, Tight-binding Hamiltonian have the form:

$$H^{TNN}(\mathbf{k}) = \begin{pmatrix} V_0 & V_1 & V_2 \\ V_1^* & V_{11} & V_{12} \\ V_2^* & V_{12}^* & V_{22} \end{pmatrix}, \quad (9)$$

where

$$\begin{aligned}
V_0 &= \varepsilon_1 + 2t_0(2\cos\alpha\cos\beta + \cos 2\alpha) + 2r_0(2\cos 3\alpha\cos\beta + \cos 2\beta), \\
\text{Re}[V_1] &= -2\sqrt{3}t_2\sin\alpha\sin\beta + 2(r_1 + r_2)\sin 3\alpha\sin\beta - 2\sqrt{3}u_2\sin 2\alpha\sin 2\beta, \\
\text{Im}[V_1] &= 2t_1\sin\alpha(2\cos\alpha + \cos\beta) + 2(r_1 - r_2)\sin 3\alpha\cos\beta + 2u_1\sin 2\alpha(2\cos 2\alpha + \cos 2\beta) \\
\text{Re}[V_2] &= 2t_2(\cos 2\alpha - \cos\alpha\cos\beta) - \frac{2}{\sqrt{3}}(r_1 + r_2)(\cos 3\alpha\cos\beta - \cos 2\beta) + 2u_2(\cos 4\alpha - \cos 2\alpha\cos 2\beta), \\
\text{Im}[V_2] &= 2\sqrt{3}t_1\cos\alpha\sin\beta + \frac{2}{\sqrt{3}}\sin\beta(r_1 - r_2)(\cos 3\alpha + 2\cos\beta), \\
V_{11} &= \varepsilon_2 + (t_{11} + 3t_{22})\cos\alpha\cos\beta + 2t_{11}\cos 2\alpha + 4r_{11}\cos 3\alpha\cos\beta \\
&\quad + 2(r_{11} + \sqrt{3}r_{12})\cos 2\beta + (u_{11} + 3u_{22})\cos 2\alpha\cos 2\beta + 2u_{11}\cos 4\alpha, \\
\text{Re}(V_{12}) &= \sqrt{3}(t_{22} - t_{11})\sin\alpha\sin\beta + 4r_{12}\sin 3\alpha\sin\beta + \sqrt{3}(u_{22} - u_{11})\sin 2\alpha\sin 2\beta, \\
\text{Im}[V_{12}] &= 4t_{12}\sin\alpha(\cos\alpha - \cos\beta) + 4u_{12}\sin 2\alpha(\cos 2\alpha - \cos 2\beta), \\
V_{22} &= \varepsilon_2 + (3t_{11} + t_{22})\cos\alpha\cos\beta + 2t_{22}\cos 2\alpha + 2r_{11}(2\cos 3\alpha\cos\beta + \cos 2\beta) \\
&\quad + \frac{2}{\sqrt{3}}r_{12}(4\cos 3\alpha\cos\beta - \cos 2\beta) + (3u_{11} + u_{22})\cos 2\alpha\cos 2\beta + 2u_{22}\cos 4\alpha,
\end{aligned}$$

and

$$(\alpha, \beta) = \left(\frac{1}{2}k_x a, \frac{\sqrt{3}}{2}k_y a\right), \quad (10)$$

11 additional parameters shown in table 1 obtained by fitting with FP calculation results. Due to the heavy transition-metal atom M, its Spin Orbit Coupling (SOC) can be larges. For simplicity, only the on-site contribution, namely, the $\mathbf{L}\cdot\mathbf{S}$ term from M atoms, is considered. Using the base $\{|d_{z^2}, \uparrow\rangle, |d_{xy}, \uparrow\rangle, |d_{x^2-y^2}, \uparrow\rangle, |d_{z^2}, \downarrow\rangle, |d_{xy}, \downarrow\rangle, |d_{x^2-y^2}, \downarrow\rangle\}$, the contribution of SOC to the Hamiltonian can be written as

$$H' = \lambda \mathbf{L}\cdot\mathbf{S} = \frac{\lambda}{2} \begin{pmatrix} L_z & 0 \\ 0 & -L_z \end{pmatrix}. \quad (11)$$

In which,

$$L_z = \begin{pmatrix} 0 & 0 & 0 \\ 0 & 0 & 2i \\ 0 & -2i & 0 \end{pmatrix}, \quad (12)$$

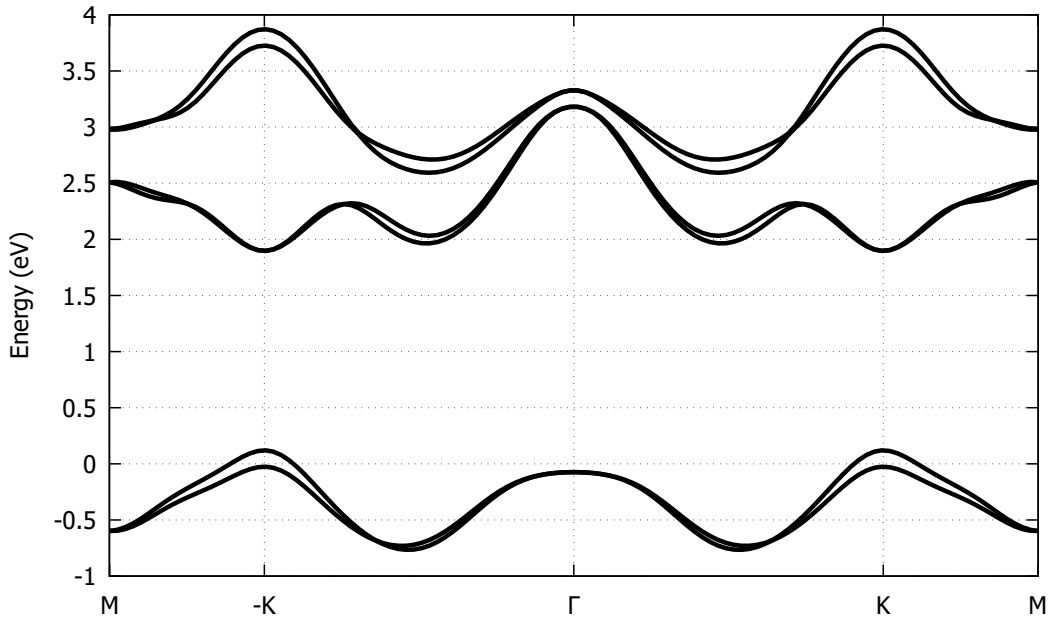
is the matrix of \hat{L}_z (z component of the orbital angular momentum) in bases of d_{z^2} , d_{xy} and $d_{x^2-y^2}$, and λ is characterized for the strength of the SOC. Under these bases, the matrix elements of \hat{L}_x and \hat{L}_y are all zeros. Therefore the Hamiltonian with SOC have the form:

$$H(\mathbf{k}) = H_{SOC}(\mathbf{k}) = I_2 \otimes H^{TNN}(\mathbf{k}) + H' = \begin{bmatrix} H(\mathbf{k}) + \frac{\lambda}{2}L_z & 0 \\ 0 & H_0(\mathbf{k}) - \frac{\lambda}{2}L_z \end{bmatrix}. \quad (13)$$

By finding eigenvalue of Hamiltonian H in each \mathbf{k} point on entire BZ, the bands structure will be obtained. The bands structure with the huge bands split at the K and K' point of MoS₂ is caused by SOC is shown in fig.2.

ε_1	ε_2	t_0	t_1	t_2	t_{11}	t_{12}	t_{22}	r_0	r_1
r_2	r_{11}	r_{12}	u_0	u_1	u_2	u_{11}	u_{12}	u_{22}	λ
0.820	1.931	-0.176	-0.101	0.531	0.084	0.169	0.070	0.070	-0.252
0.084	0.019	0.093	-0.043	0.047	0.005	0.304	-0.192	-0.162	0.073

Bảng 1: Fitting parameters in three-band tight-binding model for local-density approximation (LDA) cases for MoS_2 .¹⁷



Hình 2: Band structure of monolayer-MoS₂ along $M \rightarrow -K \rightarrow \Gamma \rightarrow K \rightarrow M$ direction, SOC causes huge splits in band-structure at K and $-K$ points.

2.3 System Hamiltonian

2.3.1 First Quantization Hamiltonian

In the present of an external electromagnetic field, the Hamiltonian for an electron in the independent electron approximation takes the form:

$$H_{1e} = \frac{(\mathbf{p} + e\mathbf{A})^2}{2m} + V_0(\mathbf{r}) - e\phi, \quad (14)$$

in which, $\mathbf{A}(\mathbf{r}, t)$ is vector potential and $\phi(\mathbf{r}, t)$ is scalar potential. With $\mathbf{p} = -i\hbar\nabla$, we expand $(\mathbf{p} + e\mathbf{A})^2 = \mathbf{p}^2 + 2e\mathbf{A}\mathbf{p} + ei\hbar\nabla(\mathbf{A}) + (e\mathbf{A})^2$. We have $\nabla \cdot (\mathbf{A}) = 0$ due to Coulomb gauge, so the (14) become

$$H_{1e} = H_{1e}^0 + \frac{e}{m}\mathbf{A} \cdot \mathbf{p} + \frac{e^2\mathbf{A}^2}{2m} - e\phi, \quad (15)$$

with H_{1e}^0 is the stationary Hamiltonian of a single electron particle:

$$H_{1e}^0 = \frac{\mathbf{p}^2}{2m} + V_0(\mathbf{r}), \quad (16)$$

and the rest is the Light-matter interaction Hamiltonian H_{1e}^{e-L} :

$$H_{1e}^{e-L} = \frac{e}{m}\mathbf{A} \cdot \mathbf{p} - e\phi + \frac{e^2\mathbf{A}^2}{2m}. \quad (17)$$

When we choose gauge $\phi = 0$, the electromagnetic field's potential relation between \mathbf{A} and ϕ becomes:

$$\mathbf{E} = -\nabla\phi - \frac{\partial\mathbf{A}}{\partial t} = -\frac{\partial\mathbf{A}}{\partial t}, \quad (18)$$

$$\mathbf{A}(\mathbf{r}, t) = -\int_{-\infty}^t dt' \mathbf{E}(\mathbf{r}, t'). \quad (19)$$

Substitute $\phi = 0$ into (15),

$$H_{1e}^{VG} = H_{1e}^0 + \frac{e}{m}\mathbf{A} \cdot \mathbf{p} + \frac{e^2\mathbf{A}^2}{2m}. \quad (20)$$

Define the velocity operator $\mathbf{v} = \frac{i}{\hbar}[H_{1e}, \mathbf{r}] = \frac{\mathbf{p} + e\mathbf{A}}{m}$, H_{1e}^{VG} will have the form

$$H_{1e}^{VG} = H_{1e}^0 + e\mathbf{A} \cdot \mathbf{v} - \frac{e^2\mathbf{A}^2}{2m}. \quad (21)$$

In velocity gauge, the light-matter interaction Hamiltonian (17) have the form:

$$H_{1e}^{e-L} = \frac{e}{m}\mathbf{A} \cdot \mathbf{p} + \frac{e^2\mathbf{A}^2}{2m}. \quad (22)$$

The electron-electron interaction between two electrons can be described by Coulomb interaction Hamiltonian:

$$H^{e-e}(\mathbf{r}_i, \mathbf{r}_j) = \frac{1}{4\pi\epsilon\epsilon_0} \frac{e^2}{|\mathbf{r}_i - \mathbf{r}_j|}, \quad (23)$$

in which the ϵ_0 is the vacuum permittivity, ϵ is relative permittivity and \mathbf{r} is the distant between two electrons, all will be in SI unit. Combine (22), (23), and (16) to have Hamiltonian for the electron system in lattice interacting with the present of an external electromagnetic field:

$$H = \sum_i H_{1e}(\mathbf{r}_i, t) = \sum_i H_{1e}^0(\mathbf{r}_i) + \sum_i H_{1e}^{e-L}(\mathbf{r}_i, t) + \frac{1}{2} \sum_{\mathbf{r}_i, \mathbf{r}_j} H^{e-e}(\mathbf{r}_i, \mathbf{r}_j). \quad (24)$$

2.3.2 Second Quantization Hamiltonian

From (24), the second quantization Hamiltonian in Bloch basics $\{|\psi_{\lambda\mathbf{k}}\rangle\}$ has the form:

$$\begin{aligned}
H &= H^0 + H^{e-L} + H^{e-e}, \\
H^0 &= \sum_{\lambda\lambda'\mathbf{k}\mathbf{k}'} \langle\psi_{\lambda\mathbf{k}}| H_{1e}^0(\mathbf{r}) |\psi_{\lambda'\mathbf{k}'}\rangle c_{\lambda\mathbf{k}}^\dagger c_{\lambda'\mathbf{k}'}, \\
H^{e-L} &= \sum_{\lambda\lambda'\mathbf{k}\mathbf{k}'} \langle\psi_{\lambda\mathbf{k}}| H^{e-L}(\mathbf{r}) |\psi_{\lambda'\mathbf{k}'}\rangle c_{\lambda\mathbf{k}}^\dagger c_{\lambda'\mathbf{k}'}, \\
H^{e-e} &= \frac{1}{2} \sum_{\mathbf{k},\mathbf{k}',\mathbf{q}} \sum_{\alpha\beta\gamma\delta} W_{\mathbf{k},\mathbf{k}',\mathbf{q}}^{\alpha\beta\gamma\delta} c_{\alpha,\mathbf{k}+\mathbf{q}}^\dagger c_{\beta,\mathbf{k}'-\mathbf{q}}^\dagger c_{\gamma,\mathbf{k}} c_{\delta,\mathbf{k}'}, \\
W_{\mathbf{k},\mathbf{k}',\mathbf{q}}^{\alpha\beta\gamma\delta} &= \langle\psi_{\alpha\mathbf{k}+\mathbf{q}} \psi_{\beta\mathbf{k}'-\mathbf{q}} | W_{ee} | \psi_{\gamma\mathbf{k}} \psi_{\delta\mathbf{k}'} \rangle,
\end{aligned} \tag{25}$$

in which the basics is orthonormal: $\langle\psi_{\lambda\mathbf{k}}|\psi_{\lambda'\mathbf{k}'}\rangle = 1$, and the creation and annihilation operators satisfied the anti-commutation relation:

$$\{c_{\lambda,\mathbf{k}}, c_{\lambda',\mathbf{k}'}\} = \{c_{\lambda,\mathbf{k}}^\dagger, c_{\lambda',\mathbf{k}'}^\dagger\} = 0, \quad \{c_{\lambda,\mathbf{k}}, c_{\lambda',\mathbf{k}'}^\dagger\} = \delta_{\lambda,\lambda'} \delta_{\mathbf{k},\mathbf{k}'}.$$
 \tag{26}

If we choosing the basics is eigenvector of H_{1e}^0 then H^0 becomes:

$$H^0 = \sum_{\lambda\mathbf{k}} \varepsilon_\lambda(\mathbf{k}) c_{\lambda\mathbf{k}}^\dagger c_{\lambda\mathbf{k}}.$$
 \tag{27}

In VG, the elements of interaction Hamiltonian matrix $\langle\psi_{\lambda\mathbf{k}}| H^{e-L}(\mathbf{r}, t) |\psi_{\lambda'\mathbf{k}'}\rangle$ is:

$$\begin{aligned}
\langle\psi_{\lambda\mathbf{k}}| H^{e-L}(\mathbf{r}, t) |\psi_{\lambda'\mathbf{k}'}\rangle &= \langle\psi_{\lambda\mathbf{k}}| \frac{e}{m} \mathbf{A}(\mathbf{r}, t) \cdot \mathbf{p} |\psi_{\lambda'\mathbf{k}'}\rangle + \frac{e^2 A^2}{2m} \delta_{\lambda\lambda'} \delta_{\mathbf{k}\mathbf{k}'} \\
&\approx \frac{e}{m} \mathbf{A}(t) \cdot \langle\psi_{\lambda\mathbf{k}}| \mathbf{p} |\psi_{\lambda'\mathbf{k}'}\rangle + \frac{e^2 A^2}{2m} \delta_{\lambda\lambda'} \delta_{\mathbf{k}\mathbf{k}'},
\end{aligned} \tag{28}$$

where

$$\begin{aligned}
\langle\psi_{\lambda\mathbf{k}}| \mathbf{p} |\psi_{\lambda'\mathbf{k}'}\rangle &= \int \frac{d^3r}{V} e^{-i\mathbf{k}\cdot\mathbf{r}} u_{\lambda\mathbf{k}}^*(\mathbf{r}) \hat{\mathbf{p}} (e^{i\mathbf{k}'\cdot\mathbf{r}} u_{\lambda'\mathbf{k}'}(\mathbf{r})) \\
&= \int \frac{d^3r}{V} e^{i(\mathbf{k}'-\mathbf{k})\cdot\mathbf{r}} u_{\lambda\mathbf{k}}^*(\mathbf{r}) (\hbar\mathbf{k} + \hat{\mathbf{p}}) u_{\lambda'\mathbf{k}'}(\mathbf{r}) \\
&= \frac{1}{N} \sum_i^N e^{i(\mathbf{k}'-\mathbf{k})\mathbf{R}_i} \int_{V_{Cell}} \frac{d^3r}{V_{Cell}} e^{i(\mathbf{k}'-\mathbf{k})\cdot\mathbf{r}} u_{\lambda\mathbf{k}}^*(\mathbf{r}) (\hbar\mathbf{k} + \hat{\mathbf{p}}) u_{\lambda'\mathbf{k}'}(\mathbf{r}).
\end{aligned} \tag{29}$$

We include the Long-wavelength approximation $\mathbf{k}', \mathbf{k} \ll \frac{2\pi}{a}$ to have:

$$\begin{aligned}
(29) &\approx \frac{1}{N} \sum_i^N e^{i(\mathbf{k}'-\mathbf{k})\mathbf{R}_i} \int_{V_{Cell}} \frac{d^3r}{V_{Cell}} u_{\lambda\mathbf{k}}^*(\mathbf{r}) (\hbar\mathbf{k}' + \hat{\mathbf{p}}) u_{\lambda'\mathbf{k}'}(\mathbf{r}) \\
&\approx \frac{1}{N} \sum_i^N e^{i(\mathbf{k}'-\mathbf{k})\mathbf{R}_i} (\hbar\mathbf{k}' \langle u_{\lambda\mathbf{k}} | u_{\lambda'\mathbf{k}'} \rangle + \langle u_{\lambda\mathbf{k}} | \hat{\mathbf{p}} | u_{\lambda'\mathbf{k}'} \rangle),
\end{aligned} \tag{30}$$

using relation $\sum_i^N e^{i(\mathbf{k}'-\mathbf{k})\mathbf{R}_i} = N\delta_{\mathbf{k}',\mathbf{k}}$ for (30) to become

$$\langle\psi_{\lambda\mathbf{k}}| \mathbf{p} |\psi_{\lambda'\mathbf{k}'}\rangle \approx (\mathbf{p}_{\lambda\lambda'}(\mathbf{k}) + \hbar\mathbf{k}\delta_{\lambda\lambda'})\delta_{\mathbf{k},\mathbf{k}'}.$$
 \tag{31}

In which

$$\mathbf{p}_{\lambda\lambda'}(\mathbf{k}) = \langle u_{\lambda\mathbf{k}} | \mathbf{p} | u_{\lambda'\mathbf{k}} \rangle. \quad (32)$$

Define $H_{1e}^0(\mathbf{k}) = e^{-i\mathbf{k}\mathbf{r}} H_{1e}^0 e^{i\mathbf{k}\mathbf{r}}$ and using the relation: $[H_{1e}^0, \mathbf{r}] = -i\frac{\hbar}{m}\mathbf{p}$ to have

$$\mathbf{p}_{\lambda\lambda'}(\mathbf{k}) = \frac{m}{\hbar} \langle u_{\lambda\mathbf{k}} | \nabla_{\mathbf{k}} H_{1e}^0(\mathbf{k}) | u_{\lambda'\mathbf{k}} \rangle. \quad (33)$$

Therefore, the light-matter interaction part of the second quantization Hamiltonian has the following form:

$$H^{e-L} = \frac{e}{m} \mathbf{A}(t) \cdot \sum_{\lambda\lambda'} \mathbf{p}_{\lambda\lambda'}(\mathbf{k}) c_{\lambda\mathbf{k}}^\dagger c_{\lambda'\mathbf{k}} + \left(\hbar\mathbf{k} + \frac{e^2 \mathbf{A}^2}{2m} \right) \sum_{\lambda\mathbf{k}} c_{\lambda\mathbf{k}}^\dagger c_{\lambda\mathbf{k}}. \quad (34)$$

The H^{e-e} derivation will be presented in Appendix B. Thus, the many-body electron system Hamiltonian in second quantization in VG have the form:

$$\begin{aligned} H &= H_{1e}^0 + H^{e-e} + H^{e-L} \\ &= \sum_{\lambda\mathbf{k}} \varepsilon_{\mathbf{k}} c_{\lambda\mathbf{k}}^\dagger c_{\lambda\mathbf{k}} \\ &\quad + \frac{1}{2} \sum_{\mathbf{k}, \mathbf{k}', \mathbf{q}} \sum_{\alpha\beta\gamma\delta} W_{\mathbf{k}, \mathbf{k}', \mathbf{q}}^{\alpha\beta\gamma\delta} c_{\alpha, \mathbf{k}+\mathbf{q}}^\dagger c_{\beta, \mathbf{k}'-\mathbf{q}}^\dagger c_{\gamma, \mathbf{k}} c_{\delta, \mathbf{k}'} \\ &\quad + \frac{e}{m} \mathbf{A}(t) \cdot \sum_{\lambda\lambda'} \mathbf{p}_{\lambda\lambda'}(\mathbf{k}) c_{\lambda\mathbf{k}}^\dagger c_{\lambda'\mathbf{k}} + \left(\hbar\mathbf{k} + \frac{e^2 \mathbf{A}^2}{2m} \right) \sum_{\lambda\mathbf{k}} c_{\lambda\mathbf{k}}^\dagger c_{\lambda\mathbf{k}}, \end{aligned} \quad (35)$$

where the Coulomb interaction matrix elements are:

$$W_{\mathbf{k}, \mathbf{k}', \mathbf{q}}^{\alpha\beta\gamma\delta} = W_{ee}(\mathbf{q}) \langle u_{\alpha\mathbf{k}+\mathbf{q}} | u_{\delta\mathbf{k}} \rangle \langle u_{\beta\mathbf{k}'-\mathbf{q}} | u_{\gamma\mathbf{k}'} \rangle, \quad (36)$$

with the 2-D Coulomb interaction in momentum space:

$$W_{ee}(\mathbf{q}) = \frac{e^2}{2\varepsilon\varepsilon_0 L^2} \frac{1}{|\mathbf{q}|}. \quad (37)$$

2.4 Semiconductor Bloch Equation

With definition of density matrix elements,

$$\rho_{\lambda\lambda'}(\mathbf{k}) = \langle c_{\lambda'\mathbf{k}}^\dagger c_{\lambda\mathbf{k}} \rangle, \quad (38)$$

we using the motion equation in Heisenberg picture for operator $c_{\lambda'\mathbf{k}}^\dagger c_{\lambda\mathbf{k}}$ and take expected value to have:

$$\frac{d}{dt} \langle c_{\lambda'\mathbf{k}}^\dagger c_{\lambda\mathbf{k}} \rangle = \frac{i}{\hbar} \langle [H, c_{\lambda'\mathbf{k}}^\dagger c_{\lambda\mathbf{k}}] \rangle. \quad (39)$$

Through the derivation in Appendix C, we have obtained the Semiconductor Bloch Equation(s) (SBE) with Coulomb interaction in the Hartree-Fock Approximation:

$$\begin{aligned} \frac{d}{dt} \rho_{\lambda\lambda'}(\mathbf{k}) &= -\frac{i}{\hbar} (\varepsilon_{\lambda}(\mathbf{k}) - \varepsilon_{\lambda'}(\mathbf{k})) \rho_{\lambda\lambda'}(\mathbf{k}) - \frac{ie}{\hbar m} \mathbf{A}(t) \sum_{\mu} [\mathbf{p}_{\lambda\mu}(\mathbf{k}) \rho_{\mu\lambda'}(\mathbf{k}) - \rho_{\lambda\mu}(\mathbf{k}) \mathbf{p}_{\mu\lambda'}(\mathbf{k})] \\ &\quad + \frac{i}{\hbar} [\Omega_{\lambda\mu}(\mathbf{k}) \rho_{\mu\lambda'}(\mathbf{k}) - \rho_{\lambda\mu}(\mathbf{k}) \Omega_{\mu\lambda'}(\mathbf{k})] + \frac{d}{dt} \rho_{\lambda\lambda'}(\mathbf{k}) \Big|_{\text{scat.}}. \end{aligned} \quad (40)$$

In which

$$\Omega_{\mu\nu}(\mathbf{k}) = \sum_{\alpha\beta\mathbf{q}} W_{\mathbf{k},\mathbf{k}+\mathbf{q},\mathbf{q}}^{\alpha\mu\beta\nu} \rho_{\alpha\beta}(\mathbf{k} + \mathbf{q}). \quad (41)$$

In (40) for the $\rho_{\lambda\lambda}(\mathbf{k})$, the density of electrons in the conduction bands and the hole densities in valence bands can be neglected due to the weak external electromagnetic field, which is also referred to as the "Low Excitation Limit"²³. Therefore,

$$\left(\frac{d}{dt} \rho(\mathbf{k}) \Big|_{\text{scat.}} \right)_{\lambda\lambda} \rightarrow 0$$

The term "interband polarization" describes the decay of quantum coherence. A common and generally accurate approximation is to use the dephasing time parameter T_2 , also known as the transverse relaxation time. This simple approximation is limited by nonlinear and non-Markovian effects, which, as mentioned earlier, can be ignored in this work. Therefore,

$$\left(\frac{d}{dt} \rho(\mathbf{k}) \Big|_{\text{scat.}} \right)_{\lambda\lambda'} \approx -\frac{\rho_{\lambda\lambda'}(\mathbf{k})}{T_2} \quad \forall \lambda \neq \lambda'. \quad (42)$$

Include above discussion into (40), we obtain the Semiconductor Bloch Equations²³:

$$\begin{aligned} \frac{d}{dt} \rho_{\lambda\lambda'}(\mathbf{k}) = & -\frac{i}{\hbar} (\varepsilon_{\lambda}(\mathbf{k}) - \varepsilon_{\lambda'}(\mathbf{k})) \rho_{\lambda\lambda'}(\mathbf{k}) - \frac{ie}{\hbar m} \mathbf{A}(t) \sum_{\mu} (\mathbf{p}_{\lambda\mu}(\mathbf{k}) \rho_{\mu\lambda'}(\mathbf{k}) - \rho_{\lambda\mu}(\mathbf{k}) \mathbf{p}_{\mu\lambda'}(\mathbf{k})) \\ & + \frac{i}{\hbar} (\Omega_{\lambda\mu}(\mathbf{k}) \rho_{\mu\lambda'}(\mathbf{k}) - \rho_{\lambda\mu}(\mathbf{k}) \Omega_{\mu\lambda'}(\mathbf{k})) - \frac{1}{T_2} \rho_{\lambda\lambda'}(\mathbf{k}) (1 - \delta_{\lambda\lambda'}), \end{aligned} \quad (43)$$

where

$$\Omega_{\mu\nu}(\mathbf{k}) = \sum_{\alpha\beta\mathbf{q}} W_{\mathbf{k},\mathbf{k}+\mathbf{q},\mathbf{q}}^{\alpha\mu\beta\nu} \rho_{\alpha\beta}(\mathbf{k} + \mathbf{q}) \quad (44)$$

2.5 Polarization Density

Polarization density is calculated from the trace of dipole and density matrix multiplication

$$\mathbf{P}(t) = \frac{e}{L^2} \sum_{\mathbf{k}} \text{Tr} \left[\vec{\xi}(\mathbf{k}) \rho(\mathbf{k}, t) \right] = \frac{e}{L^2} \sum_{\lambda\lambda'\mathbf{k}} \vec{\xi}_{\lambda\lambda'}(\mathbf{k}) \rho_{\lambda'\lambda}(\mathbf{k}, t). \quad (45)$$

Take the sum over all \mathbf{k} -points in the first BZ in 2D \mathbf{k} -grid through the integral

$$\sum_{\mathbf{k}} \dots \rightarrow \frac{L^2}{(2\pi)^2} \int_{\text{BZ}} d^2k \dots \quad (46)$$

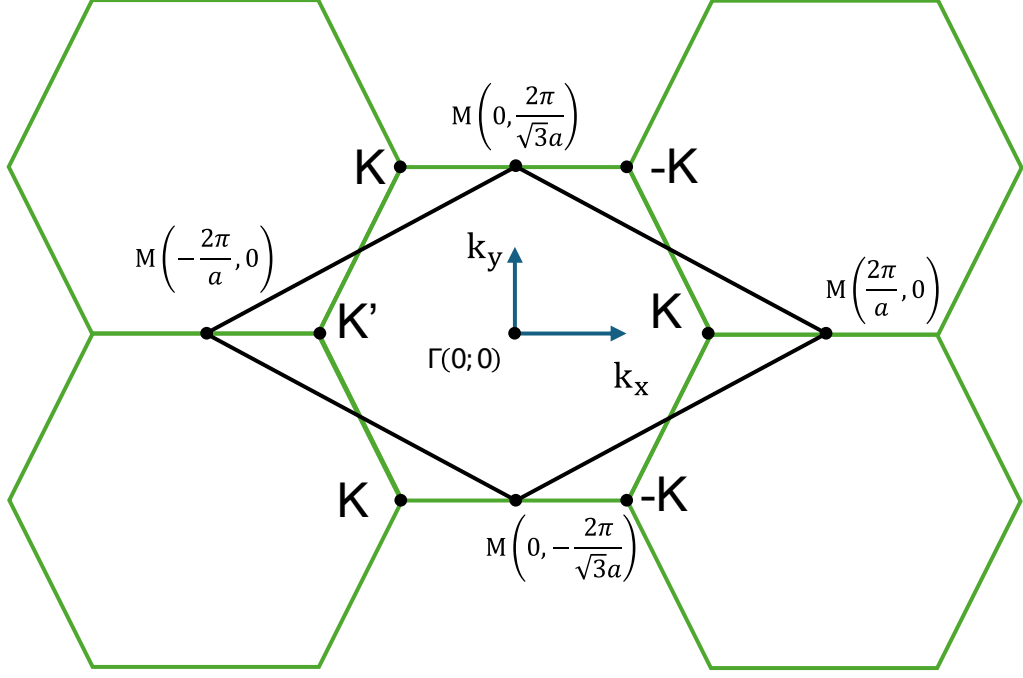
Include it into polarization density (45) to have:

$$\mathbf{P}(t) = \frac{e}{L^2} \sum_{\mathbf{k}} \text{Tr} \left[\vec{\xi}(\mathbf{k}) \rho(\mathbf{k}, t) \right] = \frac{1}{(2\pi)^2} \sum_{\lambda\lambda'} \int \vec{\xi}_{\lambda\lambda'}(\mathbf{k}) \rho_{\lambda'\lambda}(\mathbf{k}, t) d\mathbf{k}, \quad (47)$$

in which the dipole $\vec{\xi}_{\lambda\lambda'}(\mathbf{k})$ can be calculated through $\vec{p}_{\lambda\lambda'}(\mathbf{k})$ as derived in appendix D:

$$\vec{\xi}_{\lambda\lambda'}(\mathbf{k}) = -\frac{i\hbar}{m} \frac{\vec{p}_{\lambda\lambda'}(\mathbf{k})}{\varepsilon_{\lambda}(\mathbf{k}) - \varepsilon_{\lambda'}(\mathbf{k})}. \quad (48)$$

The Numerical result will be taken by using the Riemann Sum Integral.



Hình 3: Rhombus primitive unit cell construct through four M-Points, it have the same Area as first the Brillouin zone (the green Hexagon bounded with "K-point" and "K'-point")

3 Numerical Methods

3.1 Numerical Sum Over k-Space

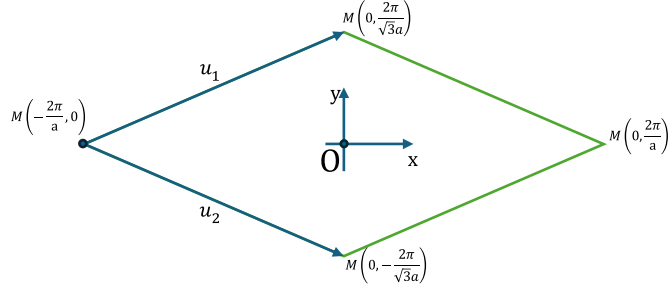
Monolayer TMD's actual lattice, denoted as MX_2 , possesses the $D3h$ point-group symmetry, as illustrated in Figure 1. The 2D first Brillouin zone takes on the shape of a hexagon. This study concentrates on the linear abortion spectrum, a feature that relies heavily on the k-points with the direct band gap of this material. To numerical calculate the eq. (47), we need to take numerical integral over the first BZ, which is inconvenient when working with the hexagon shape. Furthermore, a direct band gap is observed at the K and K' points in the first BZ, as depicted in fig. (2). There are three K and three K' points situated at the edge of the first BZ as shown in fig. 3, with each points being shared between three BZ. Consequently, we need to calculate the average numerical position by adding up the positions and then dividing by the number of points, which can pose further challenges for the many-body problems we are addressing.

To address this, we introduce the use of the rhombus primitive cell, as shown in Figure 3. This cell is constructed from 4 M-points located between K and K' on the edge of the hexagon, enabling us to focus on the properties of K and K' points both individually and in pairs.

In order to establish a new coordinate system, we will utilize the two unit vectors located at the left corner of the rhombus u_1, u_2 as shown in fig. 4, which will be reference to as the "Rhombus basics" hereinafter. To change coordinate of a point which has coordinate (v_1, v_2) in Rhombus basics into coordinate (x, y) in Cartesian Oxy basics and vice versa, we will use the transformation matrix:

$$\begin{pmatrix} x \\ y \end{pmatrix} = \frac{2\pi}{a} \left[\begin{pmatrix} 1 & 1 \\ \frac{1}{\sqrt{3}} & -\frac{1}{\sqrt{3}} \end{pmatrix} \begin{pmatrix} v_1 \\ v_2 \end{pmatrix} - \begin{pmatrix} 1 \\ 0 \end{pmatrix} \right] \quad (49)$$

Since the coordinate system Ou_1u_2 is a continuous variable, we need to convert it into discrete coordinates in order to proceed with a numerical solution. To do this, we divide the vectors u_1 and



Hình 4: New Basics Based on the rhombus unit vectors

u_2 into nk equal segments, which are then labeled as nk_1 and nk_2 , respectively.

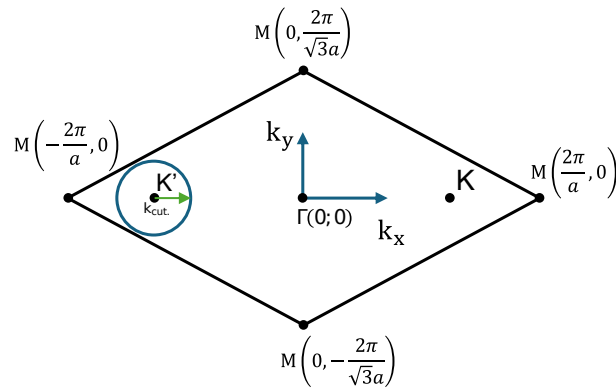
For a point label as (nk_1, nk_2) in discrete coordinate, its coordinate in Cartesian basics (x, y) can be obtain by:

$$\begin{pmatrix} x \\ y \end{pmatrix} = \frac{2\pi}{n_k a} \begin{pmatrix} 1 & 1 \\ \frac{1}{\sqrt{3}} & -\frac{1}{\sqrt{3}} \end{pmatrix} \begin{pmatrix} nk_1 \\ nk_2 \end{pmatrix} - \frac{2\pi}{a} \begin{pmatrix} 1 \\ 0 \end{pmatrix} \quad (50)$$

3.2 Cut Off K-point Technique

In our research, we are focusing on the transition between the valence and conduction bands around the K and K' points. We achieve this by using a small-intensity electric field and limiting the photon energy to extract the band gap E_{gap} . However, the calculation of the Coulomb interaction for every point in the Rhombus with other points all over the Rhombus is not efficient in terms of time cost, and convergence. As demonstrated in the 2-D Coulomb interaction equation (37), the Coulomb potential is inversely proportional to the distance between two points in k-space. To address this issue, we are introducing a technique to limit the points taken into account in the Coulomb interaction part.

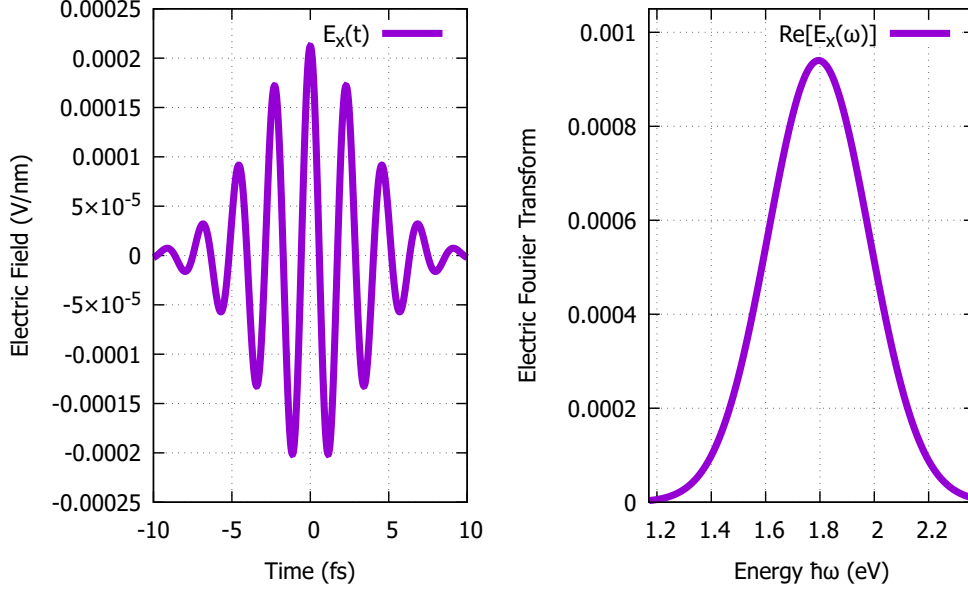
In the diagram shown in figure 5, a circle is drawn around the K' point with a radius of k_{cut} .



Hình 5: k-radius show the cutoff circle around K' points

When calculating the equation (43) at a k-point, if this k-point is outside the circle, we use

$$\Omega_{\mu\nu}(\mathbf{k}) = 0 \quad \forall \mu, \nu.$$



Hình 6: Electric field on Ox direction and it Fourier Transform

However, if the k -point is inside the circle, we will only consider interactions with other points that are also inside the circle.

In summary, we approximate the Coulomb interaction matrix elements:

$$W_{\mathbf{k},\mathbf{k}',\mathbf{q}}^{\alpha\mu\beta\nu} \approx W_{\mathbf{k},\mathbf{k}',\mathbf{q}}^{\alpha\mu\beta\nu} \theta(k_{cut.} - |\mathbf{k} - \mathbf{k}_{K'}|) \theta(k_{cut.} - |\mathbf{k}' - \mathbf{k}_{K'}|).$$

Where $\theta(k)$ is the Heaviside function, the Coulomb interaction is excluded if either point is inside the circle. The same process applies for the K point.

3.3 Numerical Analyzing

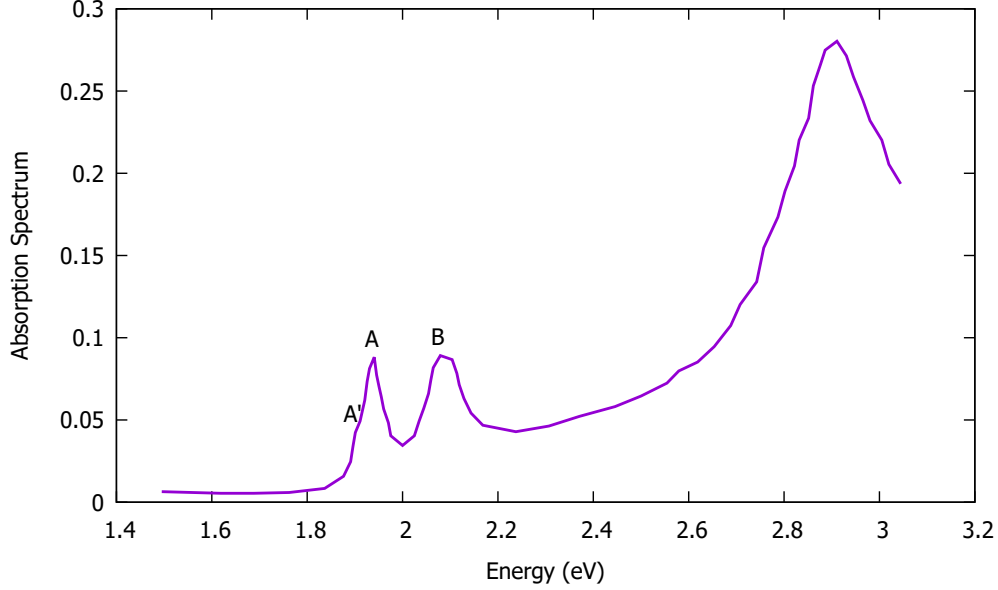
The linear absorption spectrum is determined by²³

$$\alpha(\omega) \propto \text{Im} \left\{ \frac{P(\omega)}{E(\omega)} \right\}. \quad (51)$$

In which $\mathbf{P}(\omega) = \int_{-\infty}^{\infty} \mathbf{P}(t) e^{i\omega t} dt$ and $\mathbf{E}(\omega) = \int_{-\infty}^{\infty} \mathbf{E}(t) e^{i\omega t} dt$ is Fourier transform for polarization density and Electric field. This integral can be approximated using a Riemann sum with the cutoff point by using condition $\mathbf{E}(t_{cutoff}) \lesssim 10^{-6} |\max \mathbf{E}(t)|$ and $\mathbf{P}(t_{cutoff}) \lesssim 10^{-6} |\max \mathbf{P}(t)|$. In this work, we are using the electric field in form of Gaussian wave:

$$\mathbf{E}(t) = E_0 e^{-\frac{t^2}{\tau_L^2}} (\cos(\omega_0 t), 0), \quad (52)$$

with the E_0 is the maximal amplitude, $\hbar\omega_0 = E_{\text{gap}}$, τ_L is the duration of the Gaussian pulse, and t is time, all will be calculated in SI units. The $E_x(t)$ and it Fourier transform shape shown in fig. 6.



Hình 7: Measure Absorption Spectrum of MoS₂ at $T = 5K$ extracted from¹⁰, two Exciton resonances labeled by A and B, and small trion peak labeled with A'.

4 Results and Discussion

In a previous study¹⁰, the absorption spectrum of MoS₂ at $T = 5K$ was measured and presented in figure 7. The results revealed two exciton resonances labeled as A and B, which were observed at energy levels of 1.9 and 2.1 eV, respectively. Additionally, a small trion peak was observed before the A peak. The splitting between the exciton and trion absorption peaks was approximately 34 meV at 5K.

When solving the semiconductor Bloch equations (SBE) numerically, we utilize the external electric field as follows: $E_0 = \frac{3}{\sqrt{2}} \times 10^3$ V/cm, $\hbar\omega_0 = E_{\text{gap}} = 1.77$ eV, time step $\Delta t = 0.02$ fs, $T_2 = 20(f s^{-1})$, and cutoff the Coulomb interaction at 3.0 nm^{-1} around K and K' points to simplify the calculation. By simulating with the given parameters, we observe that the density of electrons in the conduction band after the external field passes is relatively small compared to the initial electron density in the valence band ($1.10^7 \text{ cm}^{-2} \ll 1.10^{11} \text{ cm}^{-2}$), which confirms our discussion on the neglect of electron-electron scattering in equation (43). We perform Fourier transforms of energies from above and below the band gap by 1 eV. There are three main parameters we can adjust to obtain results that agree with or predict recent or future measurements: dielectric ϵ , T_2 parameter, and the number of k points on the k grid.

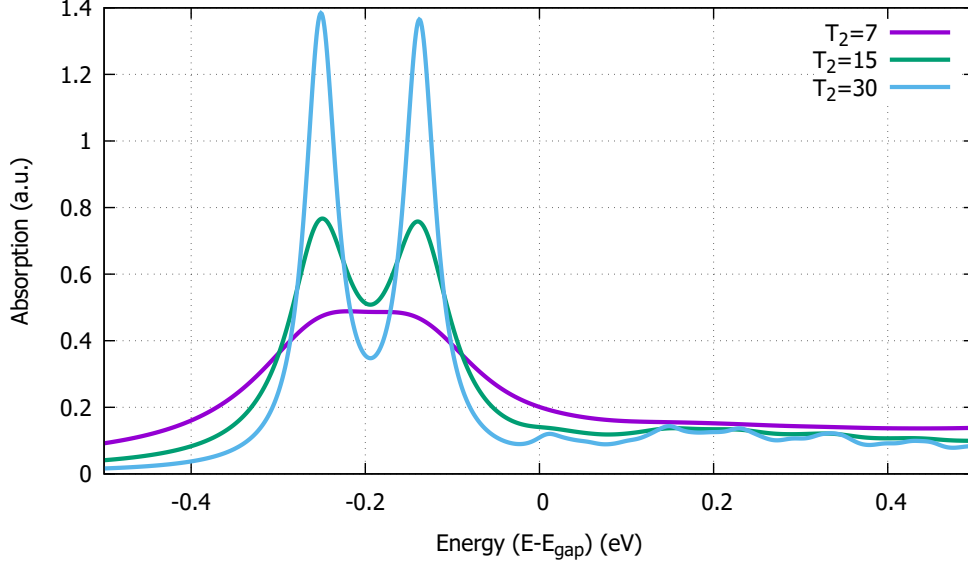
In Figure 8, our results for calculating the Absorption Spectrum with LDA parameters are presented, where the dielectric constant is $\epsilon = 2.5$ and the difference dephasing parameter is T_2 . As T_2 increases, two main peaks become clearer at 1.528 and 1.640 eV, indicating a binding energy of approximately 0.25 eV.

We present our results for calculating the Absorption Spectrum using the LDA parameter and the difference dielectric ϵ in Figure 9. As the dielectric constant ϵ increases, two main peaks shift to the left, which can be used to determine the fitting value with the experiment, the exciton binding energy result vary on dielectric parameter ϵ shown in table 2.

In Figure 10, we present our calculated results with varying numbers of k-grid points, using a dielectric constant of $\epsilon = 2.5$ to demonstrate the convergence of the results. The calculations converge

ε	1.0	1.5	2.0	2.5
$E_{\text{bind.}}(eV)$	0.95	0.55	0.36	0.25

Bảng 2: Exciton binding energy with difference dielectric ε

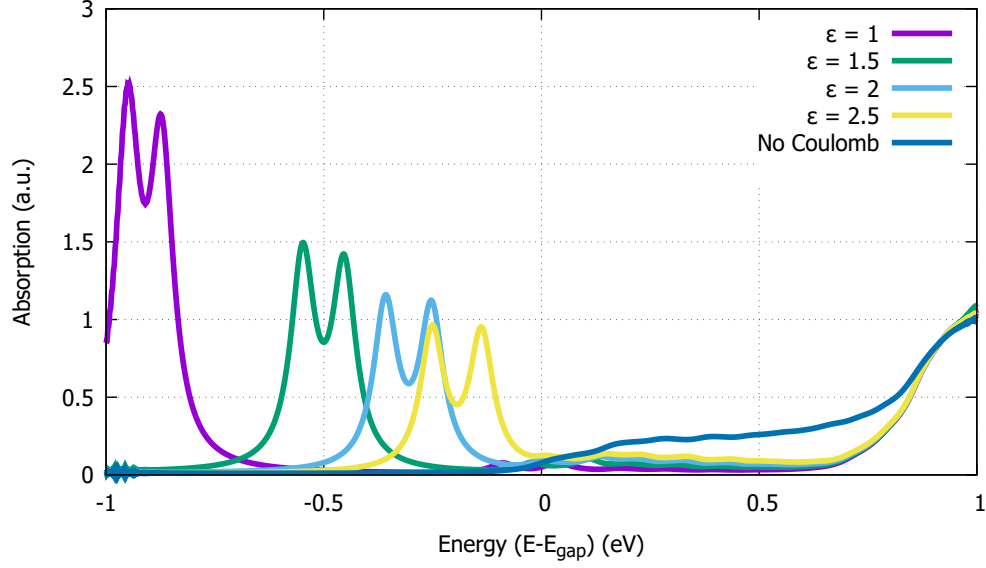


Hình 8: Absorption Spectrum with difference T_2

when the value of nk is between 60 and 120. To strike a balance between precision and time cost, we opt for $nk = 60$ for the subsequent calculations.

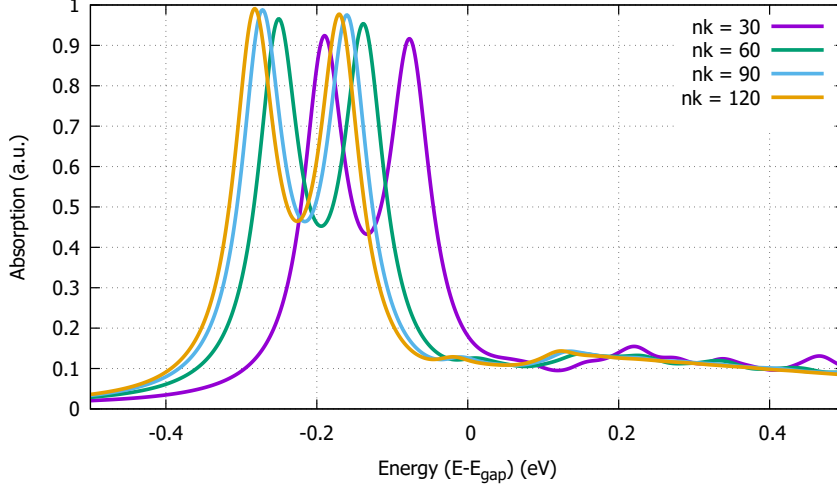
With a small T_2 of 15 (fs), the results in fig. 8 have already shown two main exciton peaks in comparison with the experimental results in fig. 7. However, as the T_2 increases at the cost of simulation time, we can see smaller exciton peaks in the absorption spectrum, as described in fig. 8. These A and B exciton resonances involve the conduction band and two valence bands (split due to spin-orbit coupling) near the K and $-K$ points, as shown in the band structure in fig. 2, providing evidence for the good approximation of the transverse relaxation time T_2 . In our results shown in Fig. 8 and the experiment by Zhang et al.¹⁰ in Fig. 7, we observed that the energy peak does not align with the expected value for the dielectric constant $\varepsilon = 2.5$. As per the data in Fig. 7¹⁰, the exciton peaks are situated at 1.9 and 2.1 eV, while in our calculations, the two peaks are at 1.528 and 1.640 eV, indicating a binding energy of the exciton of about 0.25 eV. If we only consider the distance from the band gap, our result is smaller than some previous calculations predicting the binding energy between 0.5 eV to 1 eV^{11–14}. This result agrees with more precise calculations and measurements^{9;10;24}. The difference in band gap energy can be attributed to the use of DFT calculations in our model¹⁷. This model does not consider the band gap shift caused by the underlying layers and temperature variations in the experimental measurement. The absence of the trion peak in Figure 1 is due to the trion involving an interaction between three particles (2 holes and 1 electron for a positive trion, 1 hole and 2 electrons for a negative trion), which is not included in the Hartree-Fock approximation. To observe the trion peak, it is suggested to go beyond the HFA in established equations.

This model is effective and has advantages for calculation over BZ, but it also has disadvantages and requires denser k-grids for results to converge (as shown in Fig. 10) compared to DFT models or parabola approximation models. The Bare Coulomb interaction works well in calculating the linear



Hình 9: Absorption Spectrum with difference dielectric ε and without Coulomb interaction

absorption spectrum, but for a more realistic case, the shield Coulomb interaction must be taken into account^{25;26}, especially when we want to go beyond the small excitation limit. It's worth noting that the parameter T_2 is proved to be a good approximation without requiring further techniques in showing two main exciton peaks and predicting other smaller peaks. However, for a more realistic representation, the T_2 approximation can also be expanded in terms of electron-electron and electron-phonon scattering terms, which would provide a more comprehensive analysis of the system under consideration. Additionally, it is crucial to consider the implications of these findings in the context of practical applications and the broader theoretical framework.



Hình 10: Absorption Spectrum with difference number of k-points

5 Conclusion and Further

In our research, we calculated the linear absorption of monolayer MoS₂ using a Tight-Binding three-band model with spin orbit coupling through semiconductor Bloch equations in Hartree-Fock approximation. We varied various parameters to analyze their relationship with the absorption spectrum and found that the results align with other calculations, indicating a significant binding energy up to two magnitude in comparison with other bulk semiconductors.

We did encounter some limitations, like the time-consuming process of enhancing the k-grid for better convergence and the discrepancy in the bandgap position as compared to experimental data. We also observed that the bare Coulomb interaction might not be adequate for an accurate depiction and should be fine-tuned for better outcomes.

For further researches, we can utilize this three-band tight-binding model to calculate other optoelectronic phenomena affected by excitons, such as high harmonic generation (HHG), high-order sideband generation (HSG), and photovoltaic current. When calculating the photovoltaic effect, it's important to consider the influence of Coulomb interactions. Without the consideration of Coulomb interactions, only the shift current is apparent, as we've calculated the current tensors as per ref. ²⁷. However, once we include the Coulomb interaction, the ballistic current becomes significant, and the shift tensor current is also affected. It's crucial to account for Coulomb interactions to obtain a realistic picture of the photovoltaic effect.

Appendices

A Electromagnetic Field - Charge Interaction Hamiltonian

From classical Electromagnetic Interaction, we derive the Interaction Hamiltonian between an electric charge and a classical/semi-classical electromagnetic field. The Coulomb's force and Lorentz's force for an electric charge in an electromagnetic field have the following form:

$$\vec{F} = q(\vec{E} + \vec{v} \times \vec{B}). \quad (53)$$

From Euler-Largrange equation, we have

$$\vec{F} = -\vec{\nabla}U + \frac{d}{dt}\left(\frac{\partial U}{\partial \vec{v}}\right), \quad (54)$$

To satisfied (54), U must be

$$U = q(\phi - \vec{v} \cdot \vec{A}). \quad (55)$$

From it, we can construct the Largrangian of the Interaction between the electric charge and classical Electromagnetic field

$$L = T - U = \frac{1}{2}m\vec{v}^2 + q\vec{v} \cdot \vec{A} - q\phi. \quad (56)$$

Canonical momentum for the charge is

$$\vec{p} = \frac{\partial L}{\partial \vec{v}} = m\vec{v} + q\vec{A}. \quad (57)$$

From that, we can construct classical Hamiltonian for electric charge in electromagnetic field

$$H = \vec{p} \cdot \vec{v} - L = \frac{1}{2m}(\vec{p} - q\vec{A})^2 + q\phi. \quad (58)$$

To quantization Hamiltonian, we change the classical position and canonical momentum to position and canonical momentum operators, respectively

$$\vec{p} \longrightarrow \hat{p}, \quad \vec{r} \longrightarrow \hat{r},$$

include this into (58) to get Hamiltonian operator:

$$\hat{H} = \frac{1}{2m}(\hat{p} - q\vec{A})^2 + q\phi \quad (59)$$

To confirm the Gauge variant of Schrödinger equation, we can start from it

$$i\hbar \frac{\partial}{\partial t} \psi = \hat{H} \psi = \left[\frac{1}{2m}(\hat{p} - q\vec{A})^2 + q\phi \right] \psi. \quad (60)$$

Doing Gauge transform for the electromagnetic field and phase transform for the wave function

$$\vec{A} \longrightarrow \vec{A} - \vec{\nabla}\chi, \quad \phi \longrightarrow \phi + \frac{\partial \chi}{\partial t}, \quad \psi \longrightarrow e^{-i\frac{q}{\hbar}\chi} \psi,$$

include it into (60) to get

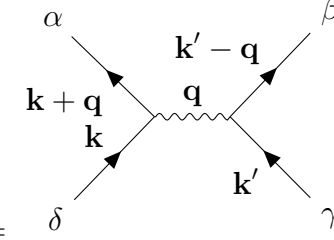
$$i\hbar \frac{\partial}{\partial t} e^{-i\frac{q}{\hbar}\chi} \psi = \left[\frac{1}{2m}(\hat{p} - q(\vec{A} - \vec{\nabla}\chi))^2 + q(\phi + \frac{\partial \chi}{\partial t}) \right] e^{-i\frac{q}{\hbar}\chi} \psi.$$

B Electron - Electron Interaction Hamiltonian

In this section, we will derive Hamiltonian for charge system in second quantization. Starting from Hamiltonian

$$H = \sum_{\mathbf{k}} \varepsilon_{\mathbf{k}} c_{\mathbf{k}}^{\dagger} c_{\mathbf{k}} + \frac{1}{2} \sum_{\mathbf{k}, \mathbf{k}', \mathbf{q}} \sum_{\alpha \beta \gamma \delta} W_{\mathbf{k}, \mathbf{k}', \mathbf{q}}^{\alpha \beta \gamma \delta} c_{\alpha, \mathbf{k} + \mathbf{q}}^{\dagger} c_{\beta, \mathbf{k}' - \mathbf{q}}^{\dagger} c_{\gamma, \mathbf{k}} c_{\delta, \mathbf{k}'} \quad (61)$$

the Coulomb matrix elements is



$$W_{\mathbf{k}, \mathbf{k}', \mathbf{q}}^{\alpha \beta \gamma \delta} = \langle \psi_{\alpha, \mathbf{k} + \mathbf{q}} \psi_{\beta, \mathbf{k}' - \mathbf{q}} | W_{ee} | \psi_{\gamma, \mathbf{k}} \psi_{\delta, \mathbf{k}'} \rangle =$$

$$= \int \frac{d^3 r}{V} \int \frac{d^3 r'}{V} e^{-i\mathbf{q}(\mathbf{r} - \mathbf{r}')} u_{\alpha, \mathbf{k} + \mathbf{q}}^*(\mathbf{r}) u_{\beta, \mathbf{k}' - \mathbf{q}}^*(\mathbf{r}') V_{ee}(\mathbf{r} - \mathbf{r}') u_{\gamma, \mathbf{k}}(\mathbf{r}) u_{\delta, \mathbf{k}'}(\mathbf{r}'), \quad (62)$$

with

$$W_{ee}(\mathbf{r}) = \frac{e^2}{4\pi\epsilon\epsilon_0} \frac{1}{|\mathbf{r}|}, \quad (63)$$

we expand it using Fourier transform

$$\begin{aligned} W_{ee}(\mathbf{q}) &= \int \frac{d^3 \mathbf{r}}{V} W_{ee}(\mathbf{r}) e^{-i\mathbf{q} \cdot \mathbf{r}} = \frac{e^2}{4\pi\epsilon\epsilon_0 V} \int d^3 \mathbf{r} \frac{1}{|\mathbf{r}|} e^{-i\mathbf{q} \cdot \mathbf{r}} \\ &= \frac{e^2}{4\pi\epsilon\epsilon_0 V} \int_0^\infty \int_0^{2\pi} \int_{-\pi}^\pi \frac{1}{r} r^2 e^{-iqr \cos(\theta)} dr d\varphi \cos(\theta) d\theta \\ &= \frac{e^2}{2\epsilon\epsilon_0 V} \int_0^\infty \int_{-1}^1 r dr d\cos\theta e^{iqr \cos\theta} = -\frac{i}{q} \frac{e^2}{2\epsilon\epsilon_0 V} \int_0^\infty dr (e^{iqr} - e^{-iqr}) \\ &= -\frac{i}{q} \frac{e^2}{2\epsilon\epsilon_0 V} \lim_{\gamma \rightarrow 0} \int_0^\infty dr (e^{iqr} - e^{-iqr}) e^{-\gamma r} \\ &= \frac{e^2}{2\epsilon\epsilon_0 V} \lim_{\gamma \rightarrow 0} \left(\int_0^\infty \frac{e^{(iq-\gamma)r}}{iq-\gamma} dr - \int_0^\infty \frac{e^{-(iq+\gamma)r}}{iq+\gamma} dr \right) = \frac{e^2}{\epsilon\epsilon_0 V} \frac{1}{q^2}. \end{aligned} \quad (64)$$

Include (64) into (62) through reverse Fourier transform

$$\begin{aligned} W_{ee}(\mathbf{r}) &= \sum_{\mathbf{q}} W_{ee}(\mathbf{q}) e^{i\mathbf{q} \cdot \mathbf{r}} = \sum_{\mathbf{q}_{||}, \mathbf{q}_{\perp}} \frac{e^2}{\epsilon\epsilon_0 V} \frac{1}{\mathbf{q}_{||}^2 + q_{\perp}^2} e^{i\mathbf{q}_{||} \cdot \mathbf{r}_{||}} e^{iq_{\perp} r_{\perp}} \\ &= \sum_{\mathbf{q}_{||}} \frac{1}{2\pi/L_z} \frac{e^2}{\epsilon\epsilon_0 V} e^{i\mathbf{q}_{||} \cdot \mathbf{r}_{||}} \int dq_{\perp} \frac{e^{iq_{\perp} r_{\perp}}}{\mathbf{q}_{||}^2 + q_{\perp}^2}, \end{aligned} \quad (65)$$

$$\begin{aligned} \bullet \int_{-\infty}^{\infty} dx \frac{e^{iax}}{a^2 + x^2} &= \oint dz \frac{e^{iaz}}{(z+ia)(z-ia)} = 2\pi i \text{Res}_{z=ia} \left[\frac{e^{iaz}}{(z+ia)(z-ia)} \right] \\ &= 2\pi i \lim_{z \rightarrow ia} \frac{e^{iaz}}{(z+ia)(z-ia)} (z-ia) = 2\pi i \frac{e^{-ax}}{2ia} = \frac{\pi e^{-ax}}{a} \quad (a > 0) \end{aligned} \quad (66)$$

$$\Rightarrow (65) = \sum_{\mathbf{q}_{||}} \frac{e^2}{2\epsilon\epsilon_0 V_{||}} e^{i\mathbf{q}_{||} \cdot \mathbf{r}_{||}} \frac{e^{-|\mathbf{q}_{||}| |\mathbf{r}_{\perp}|}}{|\mathbf{q}_{||}|} = \sum_{\mathbf{q}_{||}} W_{||}^{2D}(\mathbf{q}_{||}, \mathbf{r}_{\perp}) e^{i\mathbf{q}_{||} \cdot \mathbf{r}_{||}} \quad (67)$$

$$\therefore W_{||}^{2D}(\mathbf{q}_{||}, z) = \frac{e^2}{2\varepsilon\varepsilon_0 V_{||}} \frac{e^{-|\mathbf{q}_{||}|z}}{|\mathbf{q}_{||}|}. \quad (68)$$

Include (68) back into (62) through (67) for 2D-case

$$\begin{aligned} W_{\mathbf{k}, \mathbf{k}', \mathbf{q}}^{\alpha\beta\gamma\delta} &= \int \int d\mathbf{r}_1 d\mathbf{r}_2 u_{\mathbf{k}_{||}+\mathbf{q}_{||}}^{\alpha\dagger}(\mathbf{r}_1) u_{\mathbf{k}'_{||}-\mathbf{q}_{||}}^{\beta\dagger}(\mathbf{r}_2) V^{3D}(\mathbf{r}_2 - \mathbf{r}_1) e^{i\mathbf{q}_{||}(\mathbf{r}_2-\mathbf{r}_1)} u_{\mathbf{k}'_{||}}^{\gamma}(\mathbf{r}_2) u_{\mathbf{k}_{||}}^{\delta}(\mathbf{r}_1) \\ &= \frac{e^2}{2\varepsilon\varepsilon_0 V_{||}} \sum_{\mathbf{q}'_{||}} \int \int d\mathbf{r}_1 d\mathbf{r}_2 u_{\mathbf{k}_{||}+\mathbf{q}_{||}}^{\alpha\dagger}(\mathbf{r}_1) u_{\mathbf{k}'_{||}-\mathbf{q}_{||}}^{\beta\dagger}(\mathbf{r}_2) e^{i\mathbf{q}'_{||}(\mathbf{r}_2-\mathbf{r}_1)} \frac{e^{-|\mathbf{q}'_{||}|z_2-z_1}}{|\mathbf{q}'_{||}|} e^{i\mathbf{q}_{||}(\mathbf{r}_2-\mathbf{r}_1)} u_{\mathbf{k}'_{||}}^{\gamma}(\mathbf{r}_2) u_{\mathbf{k}_{||}}^{\delta}(\mathbf{r}_1), \end{aligned} \quad (69)$$

We take the limit $z_1, z_2 \rightarrow 0$, therefore the $W_{\mathbf{k}, \mathbf{k}', \mathbf{q}}^{\alpha\beta\gamma\delta}$ take the form:

$$W_{\mathbf{k}, \mathbf{k}', \mathbf{q}}^{\alpha\beta\gamma\delta} = \frac{e^2}{2\varepsilon\varepsilon_0 V_{||}} \sum_{\mathbf{q}} \frac{1}{|\mathbf{q}|} \langle u_{\mathbf{k}+\mathbf{q}}^{\alpha} | u_{\mathbf{k}}^{\delta} \rangle \langle u_{\mathbf{k}'-\mathbf{q}}^{\beta} | u_{\mathbf{k}'}^{\gamma} \rangle \quad (70)$$

C Motion Equation

We consider Hamiltonian (35), using Heisenberg motion equation part by part with creation and annihilation operator satisfies (26):

$$\begin{aligned}
\left[H_{1e}^0, c_{\alpha\mathbf{k}}^\dagger c_{\beta\mathbf{k}} \right] &= \sum_{\mathbf{k}'\lambda} \varepsilon_{\lambda,\mathbf{k}'} \left[c_{\lambda\mathbf{k}'}^\dagger c_{\lambda\mathbf{k}'} c_{\alpha\mathbf{k}}^\dagger c_{\beta\mathbf{k}} \right] \\
&= \sum_{\mathbf{k}'\lambda} \varepsilon_{\lambda,\mathbf{k}'} (c_{\lambda\mathbf{k}'}^\dagger c_{\lambda\mathbf{k}'} c_{\alpha\mathbf{k}}^\dagger c_{\beta\mathbf{k}} - c_{\alpha\mathbf{k}}^\dagger c_{\beta\mathbf{k}} c_{\lambda\mathbf{k}'}^\dagger c_{\lambda\mathbf{k}'}) \\
&= \sum_{\mathbf{k}\lambda'} \varepsilon_{\lambda,\mathbf{k}} (c_{\lambda\mathbf{k}}^\dagger \delta_{\lambda\alpha} \delta_{\mathbf{k}\mathbf{k}'} c_{\beta\mathbf{k}} - c_{\lambda\mathbf{k}}^\dagger c_{\alpha\mathbf{k}}^\dagger c_{\lambda\mathbf{k}'} c_{\beta\mathbf{k}} - c_{\alpha\mathbf{k}}^\dagger \delta_{\beta\lambda} \delta_{\mathbf{k}\mathbf{k}'} c_{\lambda\mathbf{k}'} + c_{\alpha\mathbf{k}}^\dagger c_{\lambda\mathbf{k}'}^\dagger c_{\beta\mathbf{k}} c_{\lambda\mathbf{k}'}) \\
&= \sum_{\mathbf{k}\lambda'} \varepsilon_{\lambda,\mathbf{k}} (c_{\lambda\mathbf{k}}^\dagger \delta_{\lambda\alpha} \delta_{\mathbf{k}\mathbf{k}'} c_{\beta\mathbf{k}} - \cancel{c_{\alpha\mathbf{k}}^\dagger c_{\lambda\mathbf{k}'}^\dagger c_{\beta\mathbf{k}} c_{\lambda\mathbf{k}'}} - c_{\alpha\mathbf{k}}^\dagger \delta_{\beta\lambda} \delta_{\mathbf{k}\mathbf{k}'} c_{\lambda\mathbf{k}'} + \cancel{c_{\alpha\mathbf{k}}^\dagger c_{\lambda\mathbf{k}'}^\dagger c_{\beta\mathbf{k}} c_{\lambda\mathbf{k}'}}) \\
&= (\varepsilon_\alpha(\mathbf{k}) - \varepsilon_\beta(\mathbf{k})) c_{\alpha\mathbf{k}}^\dagger c_{\beta\mathbf{k}}
\end{aligned} \tag{71}$$

$$\begin{aligned}
\left[H^{e-L}, c_{\alpha\mathbf{k}}^\dagger c_{\beta\mathbf{k}} \right] &= \sum_{\lambda\lambda'\mathbf{k}'} \mathbf{p}_{\lambda\lambda'}(\mathbf{k}') \left[c_{\lambda\mathbf{k}'}^\dagger c_{\lambda'\mathbf{k}'} c_{\alpha\mathbf{k}}^\dagger c_{\beta\mathbf{k}} \right] + \sum_{\lambda\mathbf{k}'} \left(\hbar\mathbf{k}' + \frac{e^2 A^2}{2m} \right) \left[\cancel{c_{\lambda\mathbf{k}'}^\dagger c_{\lambda\mathbf{k}'} c_{\alpha\mathbf{k}}^\dagger c_{\beta\mathbf{k}}} \right] \\
&= \sum_{\lambda\lambda'\mathbf{k}'} \mathbf{p}_{\lambda\lambda'}(\mathbf{k}') (c_{\lambda\mathbf{k}'}^\dagger c_{\lambda'\mathbf{k}'} c_{\alpha\mathbf{k}}^\dagger c_{\beta\mathbf{k}} - c_{\alpha\mathbf{k}}^\dagger c_{\beta\mathbf{k}} c_{\lambda\mathbf{k}'}^\dagger c_{\lambda'\mathbf{k}'}) \\
&= \sum_{\lambda\lambda'\mathbf{k}'} \mathbf{p}_{\lambda\lambda'}(\mathbf{k}') (c_{\lambda\mathbf{k}}^\dagger \delta_{\lambda'\alpha} \delta_{\mathbf{k}\mathbf{k}'} c_{\beta\mathbf{k}} - c_{\lambda\mathbf{k}}^\dagger c_{\alpha\mathbf{k}}^\dagger c_{\lambda'\mathbf{k}'} c_{\beta\mathbf{k}} - c_{\alpha\mathbf{k}}^\dagger \delta_{\beta\lambda} \delta_{\mathbf{k}\mathbf{k}'} c_{\lambda'\mathbf{k}'} + c_{\alpha\mathbf{k}}^\dagger c_{\lambda\mathbf{k}'}^\dagger c_{\beta\mathbf{k}} c_{\lambda'\mathbf{k}'}) \\
&= \sum_{\lambda\lambda'\mathbf{k}'} \mathbf{p}_{\lambda\lambda'}(\mathbf{k}') (c_{\lambda\mathbf{k}}^\dagger \delta_{\lambda'\alpha} \delta_{\mathbf{k}\mathbf{k}'} c_{\beta\mathbf{k}} - \cancel{c_{\lambda\mathbf{k}}^\dagger c_{\alpha\mathbf{k}}^\dagger c_{\lambda'\mathbf{k}'} c_{\beta\mathbf{k}}} - c_{\alpha\mathbf{k}}^\dagger \delta_{\beta\lambda} \delta_{\mathbf{k}\mathbf{k}'} c_{\lambda'\mathbf{k}'} + \cancel{c_{\alpha\mathbf{k}}^\dagger c_{\lambda\mathbf{k}'}^\dagger c_{\beta\mathbf{k}} c_{\lambda'\mathbf{k}'}}) \\
&= \sum_{\lambda} (\mathbf{p}_{\lambda\alpha}(\mathbf{k}) c_{\lambda\mathbf{k}}^\dagger c_{\beta\mathbf{k}} - \mathbf{P}_{\beta\lambda}(\mathbf{k}) c_{\alpha\mathbf{k}}^\dagger c_{\lambda\mathbf{k}})
\end{aligned} \tag{72}$$

$$\begin{aligned}
\left[H^{Coulomb}, c_{\lambda\mathbf{k}''}^\dagger c_{\lambda'\mathbf{k}''} \right] &= \sum_{\mathbf{k},\mathbf{k}',\mathbf{q}} \sum_{\alpha\beta\gamma\delta} W_{\mathbf{k},\mathbf{k}',\mathbf{q}}^{\alpha\beta\gamma\delta} \left[c_{\alpha,\mathbf{k}+\mathbf{q}}^\dagger c_{\beta,\mathbf{k}'-\mathbf{q}}^\dagger c_{\gamma,\mathbf{k}C\delta,\mathbf{k}'} c_{\lambda\mathbf{k}''}^\dagger c_{\lambda'\mathbf{k}''} \right] \\
&= \sum_{\mathbf{k},\mathbf{k}',\mathbf{q}} \sum_{\alpha\beta\gamma\delta} W_{\mathbf{k},\mathbf{k}',\mathbf{q}}^{\alpha\beta\gamma\delta} (c_{\alpha,\mathbf{k}+\mathbf{q}}^\dagger c_{\beta,\mathbf{k}'-\mathbf{q}}^\dagger c_{\gamma,\mathbf{k}C\delta,\mathbf{k}'} c_{\lambda\mathbf{k}''}^\dagger c_{\lambda'\mathbf{k}''} - c_{\lambda\mathbf{k}''}^\dagger c_{\lambda'\mathbf{k}''} c_{\alpha,\mathbf{k}+\mathbf{q}}^\dagger c_{\beta,\mathbf{k}'-\mathbf{q}}^\dagger c_{\gamma,\mathbf{k}C\delta,\mathbf{k}'}) \\
&\bullet \quad c_{\alpha,\mathbf{k}+\mathbf{q}}^\dagger c_{\beta,\mathbf{k}'-\mathbf{q}}^\dagger c_{\gamma,\mathbf{k}C\delta,\mathbf{k}'} c_{\lambda\mathbf{k}''}^\dagger c_{\lambda'\mathbf{k}''} = c_{\alpha,\mathbf{k}+\mathbf{q}}^\dagger c_{\beta,\mathbf{k}'-\mathbf{q}}^\dagger c_{\gamma,\mathbf{k}} \delta_{\lambda,\delta} \delta_{\mathbf{k}',\mathbf{k}''} c_{\lambda'\mathbf{k}''} - c_{\alpha,\mathbf{k}+\mathbf{q}}^\dagger c_{\beta,\mathbf{k}'-\mathbf{q}}^\dagger c_{\gamma,\mathbf{k}} c_{\lambda\mathbf{k}''}^\dagger c_{\delta,\mathbf{k}'} c_{\lambda'\mathbf{k}''} \\
&= c_{\alpha,\mathbf{k}+\mathbf{q}}^\dagger c_{\beta,\mathbf{k}'-\mathbf{q}}^\dagger c_{\gamma,\mathbf{k}} \delta_{\lambda,\delta} \delta_{\mathbf{k}',\mathbf{k}''} c_{\lambda'\mathbf{k}''} - c_{\alpha,\mathbf{k}+\mathbf{q}}^\dagger c_{\beta,\mathbf{k}'-\mathbf{q}}^\dagger \delta_{\lambda\gamma} \delta_{\mathbf{k}\mathbf{k}''} c_{\delta,\mathbf{k}'} c_{\lambda'\mathbf{k}''} + \cancel{c_{\alpha,\mathbf{k}+\mathbf{q}}^\dagger c_{\beta,\mathbf{k}'-\mathbf{q}}^\dagger c_{\lambda\mathbf{k}''}^\dagger c_{\gamma,\mathbf{k}C\delta,\mathbf{k}'} c_{\lambda'\mathbf{k}''}} \\
&\bullet \quad c_{\lambda\mathbf{k}''}^\dagger c_{\lambda'\mathbf{k}''} c_{\alpha,\mathbf{k}+\mathbf{q}}^\dagger c_{\beta,\mathbf{k}'-\mathbf{q}}^\dagger c_{\gamma,\mathbf{k}C\delta,\mathbf{k}'} = c_{\lambda\mathbf{k}''}^\dagger \delta_{\lambda',\alpha} \delta_{\mathbf{k}'',\mathbf{k}+\mathbf{q}} c_{\beta,\mathbf{k}'-\mathbf{q}}^\dagger c_{\gamma,\mathbf{k}C\delta,\mathbf{k}'} - \cancel{c_{\lambda\mathbf{k}''}^\dagger c_{\alpha,\mathbf{k}+\mathbf{q}}^\dagger c_{\lambda'\mathbf{k}''} c_{\beta,\mathbf{k}'-\mathbf{q}}^\dagger c_{\gamma,\mathbf{k}C\delta,\mathbf{k}'}} \\
&= c_{\lambda\mathbf{k}''}^\dagger \delta_{\lambda',\alpha} \delta_{\mathbf{k}'',\mathbf{k}+\mathbf{q}} c_{\beta,\mathbf{k}'-\mathbf{q}}^\dagger c_{\gamma,\mathbf{k}C\delta,\mathbf{k}'} - c_{\lambda\mathbf{k}''}^\dagger c_{\alpha,\mathbf{k}+\mathbf{q}}^\dagger \delta_{\lambda'\beta} \delta_{\mathbf{k}'',\mathbf{k}'-\mathbf{q}} c_{\gamma,\mathbf{k}C\delta,\mathbf{k}'} + \cancel{c_{\lambda\mathbf{k}''}^\dagger c_{\alpha,\mathbf{k}+\mathbf{q}}^\dagger c_{\beta,\mathbf{k}'-\mathbf{q}}^\dagger c_{\lambda'\mathbf{k}''} c_{\gamma,\mathbf{k}C\delta,\mathbf{k}'}} \\
\left[H^{Coulomb}, c_{\lambda\mathbf{k}''}^\dagger c_{\lambda'\mathbf{k}''} \right] &= \sum_{\mathbf{k},\mathbf{k}',\mathbf{q}} \sum_{\alpha\beta\gamma\delta} W_{\mathbf{k},\mathbf{k}',\mathbf{q}}^{\alpha\beta\gamma\delta} (c_{\alpha,\mathbf{k}+\mathbf{q}}^\dagger c_{\beta,\mathbf{k}'-\mathbf{q}}^\dagger c_{\gamma,\mathbf{k}} \delta_{\lambda,\delta} \delta_{\mathbf{k}',\mathbf{k}''} c_{\lambda'\mathbf{k}''} - c_{\alpha,\mathbf{k}+\mathbf{q}}^\dagger c_{\beta,\mathbf{k}'-\mathbf{q}}^\dagger \delta_{\lambda\gamma} \delta_{\mathbf{k}\mathbf{k}''} c_{\delta,\mathbf{k}'} c_{\lambda'\mathbf{k}''} \\
&\quad - c_{\lambda\mathbf{k}''}^\dagger \delta_{\lambda',\alpha} \delta_{\mathbf{k}'',\mathbf{k}+\mathbf{q}} c_{\beta,\mathbf{k}'-\mathbf{q}}^\dagger c_{\gamma,\mathbf{k}C\delta,\mathbf{k}'} + c_{\lambda\mathbf{k}''}^\dagger c_{\alpha,\mathbf{k}+\mathbf{q}}^\dagger \delta_{\lambda'\beta} \delta_{\mathbf{k}'',\mathbf{k}'-\mathbf{q}} c_{\gamma,\mathbf{k}C\delta,\mathbf{k}'})
\end{aligned}$$

$$\begin{aligned}
&= \sum_{\mathbf{k}, \mathbf{k}', \mathbf{q}} \sum_{\alpha \beta \gamma \delta} W_{\mathbf{k}, \mathbf{k}', \mathbf{q}}^{\alpha \beta \gamma \delta} c_{\alpha, \mathbf{k}+\mathbf{q}}^\dagger c_{\beta, \mathbf{k}'-\mathbf{q}}^\dagger c_{\gamma, \mathbf{k}} \delta_{\lambda, \delta} \delta_{\mathbf{k}', \mathbf{k}''} c_{\lambda' \mathbf{k}''} - \sum_{\mathbf{k}, \mathbf{k}', \mathbf{q}} \sum_{\alpha \beta \gamma \delta} W_{\mathbf{k}, \mathbf{k}', \mathbf{q}}^{\alpha \beta \gamma \delta} c_{\alpha, \mathbf{k}+\mathbf{q}}^\dagger c_{\beta, \mathbf{k}'-\mathbf{q}}^\dagger \delta_{\lambda \gamma} \delta_{\mathbf{k} \mathbf{k}''} c_{\delta, \mathbf{k}'} c_{\lambda' \mathbf{k}''} \\
&- \sum_{\mathbf{k}, \mathbf{k}', \mathbf{q}} \sum_{\alpha \beta \gamma \delta} W_{\mathbf{k}, \mathbf{k}', \mathbf{q}}^{\alpha \beta \gamma \delta} c_{\lambda \mathbf{k}''}^\dagger \delta_{\lambda', \alpha} \delta_{\mathbf{k}'', \mathbf{k}+\mathbf{q}} c_{\beta, \mathbf{k}'-\mathbf{q}}^\dagger c_{\gamma, \mathbf{k}} c_{\delta, \mathbf{k}'} + \sum_{\mathbf{k}, \mathbf{k}', \mathbf{q}} \sum_{\alpha \beta \gamma \delta} W_{\mathbf{k}, \mathbf{k}', \mathbf{q}}^{\alpha \beta \gamma \delta} c_{\lambda \mathbf{k}''}^\dagger c_{\alpha, \mathbf{k}+\mathbf{q}}^\dagger \delta_{\lambda' \beta} \delta_{\mathbf{k}'', \mathbf{k}'-\mathbf{q}} c_{\gamma, \mathbf{k}} c_{\delta, \mathbf{k}'} \\
&= \sum_{\mathbf{k}, \mathbf{q}} \sum_{\alpha \beta \gamma} W_{\mathbf{k}, \mathbf{k}'', \mathbf{q}}^{\alpha \beta \gamma \lambda} c_{\alpha, \mathbf{k}+\mathbf{q}}^\dagger c_{\beta, \mathbf{k}''-\mathbf{q}}^\dagger c_{\gamma, \mathbf{k}} c_{\lambda' \mathbf{k}''} - \sum_{\mathbf{k}', \mathbf{q}} \sum_{\alpha \beta \delta} W_{\mathbf{k}'', \mathbf{k}', \mathbf{q}}^{\alpha \beta \lambda \delta} c_{\alpha, \mathbf{k}''+\mathbf{q}}^\dagger c_{\beta, \mathbf{k}'-\mathbf{q}}^\dagger c_{\delta, \mathbf{k}'} c_{\lambda' \mathbf{k}''} \\
&- \sum_{\mathbf{k}', \mathbf{q}} \sum_{\beta \gamma \delta} W_{\mathbf{k}'', \mathbf{q}, \mathbf{k}', \mathbf{q}}^{\lambda' \beta \gamma \delta} c_{\lambda \mathbf{k}''}^\dagger c_{\beta, \mathbf{k}'-\mathbf{q}}^\dagger c_{\gamma, \mathbf{k}''-\mathbf{q}} c_{\delta, \mathbf{k}'} + \sum_{\mathbf{k}, \mathbf{q}} \sum_{\alpha \gamma \delta} W_{\mathbf{k}, \mathbf{k}', \mathbf{q}}^{\alpha \lambda' \gamma \delta} c_{\lambda \mathbf{k}''}^\dagger c_{\alpha, \mathbf{k}+\mathbf{q}}^\dagger c_{\gamma, \mathbf{k}} c_{\delta, \mathbf{k}''+\mathbf{q}} \\
&= \sum_{\mathbf{k}, \mathbf{q}} \sum_{\alpha \beta \gamma} W_{\mathbf{k}, \mathbf{k}'', \mathbf{q}}^{\alpha \beta \gamma \lambda} c_{\alpha, \mathbf{k}+\mathbf{q}}^\dagger c_{\beta, \mathbf{k}''-\mathbf{q}}^\dagger c_{\gamma, \mathbf{k}} c_{\lambda' \mathbf{k}''} - \sum_{\mathbf{k}', \mathbf{q}} \sum_{\alpha \beta \delta} W_{\mathbf{k}'', \mathbf{k}', \mathbf{q}}^{\alpha \beta \lambda \delta} c_{\alpha, \mathbf{k}''+\mathbf{q}}^\dagger c_{\beta, \mathbf{k}'-\mathbf{q}}^\dagger c_{\delta, \mathbf{k}'} c_{\lambda' \mathbf{k}''} \\
&- \sum_{\mathbf{k}', \mathbf{q}} \sum_{\beta \gamma \delta} W_{\mathbf{k}'', \mathbf{q}, \mathbf{k}', \mathbf{q}}^{\lambda' \beta \gamma \delta} c_{\lambda \mathbf{k}''}^\dagger c_{\beta, \mathbf{k}'-\mathbf{q}}^\dagger c_{\gamma, \mathbf{k}''-\mathbf{q}} c_{\delta, \mathbf{k}'} + \sum_{\mathbf{k}, \mathbf{q}} \sum_{\alpha \gamma \delta} W_{\mathbf{k}, \mathbf{k}', \mathbf{q}}^{\alpha \lambda' \gamma \delta} c_{\lambda \mathbf{k}''}^\dagger c_{\alpha, \mathbf{k}+\mathbf{q}}^\dagger c_{\gamma, \mathbf{k}} c_{\delta, \mathbf{k}''+\mathbf{q}} \\
&= 2 \sum_{\mathbf{k}' \mathbf{q}} \left(\sum_{\alpha \beta \gamma} W_{\mathbf{k}'', \mathbf{k}', \mathbf{q}}^{\alpha \beta \gamma \lambda} c_{\alpha \mathbf{k}''+\mathbf{q}}^\dagger c_{\beta \mathbf{k}'-\mathbf{q}}^\dagger c_{\gamma \mathbf{k}'} c_{\lambda' \mathbf{k}''} + W_{\mathbf{k}', \mathbf{k}''+\mathbf{q}, \mathbf{q}}^{\alpha \lambda' \gamma \delta} c_{\lambda \mathbf{k}''}^\dagger c_{\alpha \mathbf{k}'+\mathbf{q}}^\dagger c_{\gamma \mathbf{k}''+\mathbf{q}} c_{\delta \mathbf{k}'} \right) \quad (73)
\end{aligned}$$

Using approximation for the 4-operators into the form of multiplication of 2-operators (Hartree-Fock approximation):

$$\begin{aligned}
\sum_{\mathbf{k}' \mathbf{q}} \left\langle c_{\alpha \mathbf{k}''+\mathbf{q}}^\dagger c_{\beta \mathbf{k}'-\mathbf{q}}^\dagger c_{\gamma \mathbf{k}'} c_{\lambda' \mathbf{k}''} \right\rangle &= - \sum_{\mathbf{k}' \mathbf{q}} \left\langle c_{\alpha \mathbf{k}''+\mathbf{q}}^\dagger c_{\gamma \mathbf{k}'} \right\rangle \left\langle c_{\beta \mathbf{k}'-\mathbf{q}}^\dagger c_{\lambda' \mathbf{k}''} \right\rangle \delta_{\mathbf{k}' \mathbf{k}''} \\
&= - \sum_{\mathbf{q}} \left\langle c_{\alpha \mathbf{k}''+\mathbf{q}}^\dagger c_{\gamma \mathbf{k}''+\mathbf{q}} \right\rangle \left\langle c_{\mathbf{k}''}^\dagger c_{\lambda' \mathbf{k}'} \right\rangle \quad (74)
\end{aligned}$$

$$\begin{aligned}
\sum_{\mathbf{k}' \mathbf{q}} \left\langle c_{\lambda \mathbf{k}''}^\dagger c_{\alpha \mathbf{k}'+\mathbf{q}}^\dagger c_{\gamma \mathbf{k}''+\mathbf{q}} c_{\delta \mathbf{k}'} \right\rangle &= \sum_{\mathbf{k}' \mathbf{q}} \left\langle c_{\lambda \mathbf{k}''}^\dagger c_{\delta \mathbf{k}'} \right\rangle \left\langle c_{\alpha \mathbf{k}'+\mathbf{q}}^\dagger c_{\gamma \mathbf{k}''+\mathbf{q}} \right\rangle \delta_{\mathbf{k}', \mathbf{k}''} \\
&= \sum_{\mathbf{q}} \left\langle c_{\lambda \mathbf{k}''}^\dagger c_{\delta \mathbf{k}''} \right\rangle \left\langle c_{\alpha \mathbf{k}''+\mathbf{q}}^\dagger c_{\gamma \mathbf{k}''+\mathbf{q}} \right\rangle \quad (75)
\end{aligned}$$

Include HFA (74) and (75) into (73). Take all the communication term (71), (72) and (73) into (39) to get the SBE in HFA:

$$\begin{aligned}
\frac{d}{dt} \rho_{\lambda \lambda'}(\mathbf{k}) &= - \frac{i}{\hbar} (\varepsilon_{\lambda}(\mathbf{k}) - \varepsilon_{\lambda'}(\mathbf{k})) \rho_{\lambda \lambda'} - \frac{ie}{\hbar m} \mathbf{A}(t) \sum_{\mu} (\mathbf{p}_{\lambda \mu}(\mathbf{k}) \rho_{\mu \lambda'}(\mathbf{k}) - \rho_{\lambda \mu}(\mathbf{k}) \mathbf{p}_{\mu \lambda'}(\mathbf{k})) \\
&+ \frac{i}{\hbar} (\Omega_{\lambda \mu}(\mathbf{k}) \rho_{\mu \lambda'}(\mathbf{k}) - \rho_{\lambda \mu}(\mathbf{k}) \Omega_{\mu \lambda'}(\mathbf{k})) \quad (76)
\end{aligned}$$

D Dipole Matrix Elements

Starting from position matrix element:

$$\langle \psi_{\lambda \mathbf{k}} | \mathbf{r} | \psi_{\lambda' \mathbf{k}'} \rangle = \int \frac{d^3 r}{V} u_{\lambda \mathbf{k}}^*(\mathbf{r}) e^{-i \mathbf{k} \cdot \mathbf{r}} \mathbf{r} u_{\lambda' \mathbf{k}'}(\mathbf{r}) e^{i \mathbf{k}' \cdot \mathbf{r}} \quad (77)$$

$$\begin{aligned} &= i \nabla_{\mathbf{k}} \left(\int \frac{d^3 r}{V} e^{-i \mathbf{k} \cdot \mathbf{r}} u_{\lambda \mathbf{k}}^*(\mathbf{r}) u_{\lambda' \mathbf{k}'}(\mathbf{r}) e^{i \mathbf{k}' \cdot \mathbf{r}} \right) - \int \frac{d^3 r}{V} i e^{-i \mathbf{k} \cdot \mathbf{r}} (\nabla_{\mathbf{k}} u_{\lambda \mathbf{k}}^*) u_{\lambda' \mathbf{k}'} e^{i \mathbf{k}' \cdot \mathbf{r}} \\ &= i \nabla_{\mathbf{k}} \left(\frac{1}{N} \sum_i^N e^{i(\mathbf{k}' - \mathbf{k}) \cdot \mathbf{R}_i} \int_{V_{cell}} \frac{d^3 r}{V_{cell}} e^{-i \mathbf{k} \cdot \mathbf{r}} u_{\lambda \mathbf{k}}^*(\mathbf{r}) u_{\lambda' \mathbf{k}'}(\mathbf{r}) e^{i \mathbf{k}' \cdot \mathbf{r}} \right) \\ &\quad - i \frac{1}{N} \sum_i^N e^{i(\mathbf{k}' - \mathbf{k}) \cdot \mathbf{R}_i} \int_{V_{cell}} \frac{d^3 r}{V_{cell}} e^{i(\mathbf{k}' - \mathbf{k}) \cdot \mathbf{r}} (\nabla_{\mathbf{k}} u_{\lambda \mathbf{k}}^*) u_{\lambda' \mathbf{k}'}. \end{aligned} \quad (78)$$

Again, using the long-wavelength approximation to have

$$\langle \psi_{\lambda \mathbf{k}} | \mathbf{r} | \psi_{\lambda' \mathbf{k}'} \rangle \approx i \nabla_{\mathbf{k}} \delta_{\mathbf{k}, \mathbf{k}'} \delta_{\lambda \lambda'} - i \delta_{\mathbf{k}, \mathbf{k}'} \langle \nabla_{\mathbf{k}} u_{\lambda \mathbf{k}} | u_{\lambda' \mathbf{k}'} \rangle, \quad (79)$$

Define the dielectric matrix elements:

$$\xi_{\lambda \lambda'}(\mathbf{k}) = -i \langle \nabla_{\mathbf{k}} u_{\lambda \mathbf{k}} | u_{\lambda' \mathbf{k}'} \rangle, \quad (80)$$

Include this into (79) to have

$$\langle \psi_{\lambda \mathbf{k}} | \mathbf{r} | \psi_{\lambda' \mathbf{k}'} \rangle = \delta_{\mathbf{k}, \mathbf{k}'} (i \delta_{\lambda \lambda'} \nabla_{\mathbf{k}} + \xi_{\lambda \lambda'}(\mathbf{k})), \quad (81)$$

Using this relation along with (31) and $[H_{1e}^0, \mathbf{r}] = -i \frac{\hbar}{m} \mathbf{p}$ for $\lambda \neq \lambda'$:

$$\xi_{\lambda \lambda'}(\mathbf{k}) = -\frac{i \hbar}{m} \frac{\mathbf{p}_{\lambda \lambda'}(\mathbf{k})}{\varepsilon_{\lambda}(\mathbf{k}) - \varepsilon_{\lambda'}(\mathbf{k})} \quad (82)$$

Tài liệu

- [1] A. K. Geim and I. V. Grigorieva, “Van der Waals heterostructures,” *Nature*, vol. 499, pp. 419–425, July 2013. Publisher: Nature Publishing Group.
- [2] Q. H. Wang, K. Kalantar-Zadeh, A. Kis, J. N. Coleman, and M. S. Strano, “Electronics and optoelectronics of two-dimensional transition metal dichalcogenides,” *Nature Nanotechnology*, vol. 7, pp. 699–712, Nov. 2012.
- [3] J. Jiang, Z. Chen, Y. Hu, Y. Xiang, L. Zhang, Y. Wang, G.-C. Wang, and J. Shi, “Flexo-photovoltaic effect in MoS₂,” *Nature Nanotechnology*, vol. 16, pp. 894–901, Aug. 2021. Publisher: Nature Publishing Group.
- [4] B. Kim, N. Park, and J. Kim, “Giant bulk photovoltaic effect driven by the wall-to-wall charge shift in WS₂ nanotubes,” *Nature Communications*, vol. 13, p. 3237, June 2022. Publisher: Nature Publishing Group.
- [5] Y. J. Zhang, T. Ideue, M. Onga, F. Qin, R. Suzuki, A. Zak, R. Tenne, J. H. Smet, and Y. Iwasa, “Enhanced intrinsic photovoltaic effect in tungsten disulfide nanotubes,” *Nature*, vol. 570, pp. 349–353, June 2019. Publisher: Nature Publishing Group.
- [6] D. Yang, J. Wu, B. T. Zhou, J. Liang, T. Ideue, T. Siu, K. M. Awan, K. Watanabe, T. Taniguchi, Y. Iwasa, M. Franz, and Z. Ye, “Spontaneous-polarization-induced photovoltaic effect in rhombohedrally stacked MoS₂,” *Nature Photonics*, vol. 16, pp. 469–474, June 2022. Publisher: Nature Publishing Group.
- [7] D. Xiao, W. Yao, and Q. Niu, “Valley-Contrasting Physics in Graphene: Magnetic Moment and Topological Transport,” *Physical Review Letters*, vol. 99, p. 236809, Dec. 2007. Publisher: American Physical Society.
- [8] W. Yao, D. Xiao, and Q. Niu, “Valley-dependent optoelectronics from inversion symmetry breaking,” *Physical Review B*, vol. 77, p. 235406, June 2008. Publisher: American Physical Society.
- [9] E. V. Kirichenko and V. A. Stephanovich, “The influence of Coulomb interaction screening on the excitons in disordered two-dimensional insulators,” *Scientific Reports*, vol. 11, p. 11956, June 2021. Number: 1 Publisher: Nature Publishing Group.
- [10] C. Zhang, H. Wang, W. Chan, C. Manolatou, and F. Rana, “Absorption of light by excitons and trions in monolayers of metal dichalcogenide MoS_2 : Experiments and theory,” *Physical Review B*, vol. 89, p. 205436, May 2014. Publisher: American Physical Society.
- [11] A. Ramasubramaniam, “Large excitonic effects in monolayers of molybdenum and tungsten dichalcogenides,” *Physical Review B*, vol. 86, p. 115409, Sept. 2012. Publisher: American Physical Society.
- [12] D. Y. Qiu, F. H. da Jornada, and S. G. Louie, “Optical Spectrum of MoS_2 : Many-Body Effects and Diversity of Exciton States,” *Physical Review Letters*, vol. 111, p. 216805, Nov. 2013. Publisher: American Physical Society.
- [13] T. Cheiwchanchamnangij and W. R. L. Lambrecht, “Quasiparticle band structure calculation of monolayer, bilayer, and bulk MoS₂,” *Physical Review B*, vol. 85, p. 205302, May 2012. Publisher: American Physical Society.

- [14] H. Shi, H. Pan, Y.-W. Zhang, and B. I. Yakobson, “Quasiparticle band structures and optical properties of strained monolayer MoS_2 and WS_2 ,” *Physical Review B*, vol. 87, p. 155304, Apr. 2013. Publisher: American Physical Society.
- [15] L. Meckbach, J. Hader, U. Huttner, J. Neuhaus, J. T. Steiner, T. Stroucken, J. V. Moloney, and S. W. Koch, “Ultrafast band-gap renormalization and build-up of optical gain in monolayer MoTe_2 ,” *Physical Review B*, vol. 101, p. 075401, Feb. 2020.
- [16] T. C. Berkelbach, M. S. Hybertsen, and D. R. Reichman, “Theory of neutral and charged excitons in monolayer transition metal dichalcogenides,” *Physical Review B*, vol. 88, p. 045318, July 2013.
- [17] G.-B. Liu, W.-Y. Shan, Y. Yao, W. Yao, and D. Xiao, “Three-band tight-binding model for monolayers of group-VIB transition metal dichalcogenides,” *Physical Review B*, vol. 88, p. 085433, Aug. 2013. Publisher: American Physical Society.
- [18] D. Xiao, G.-B. Liu, W. Feng, X. Xu, and W. Yao, “Coupled Spin and Valley Physics in Monolayers of MoS_2 and Other Group-VI Dichalcogenides,” *Physical Review Letters*, vol. 108, p. 196802, May 2012. Publisher: American Physical Society.
- [19] L. F. Mattheiss, “Band Structures of Transition-Metal-Dichalcogenide Layer Compounds,” *Physical Review B*, vol. 8, pp. 3719–3740, Oct. 1973. Publisher: American Physical Society.
- [20] S. Lebegue and O. Eriksson, “Electronic structure of two-dimensional crystals from ab initio theory,” *Physical Review B*, vol. 79, p. 115409, Mar. 2009. Publisher: American Physical Society.
- [21] Z. Y. Zhu, Y. C. Cheng, and U. Schwingenschlögl, “Giant spin-orbit-induced spin splitting in two-dimensional transition-metal dichalcogenide semiconductors,” *Physical Review B*, vol. 84, p. 153402, Oct. 2011. Publisher: American Physical Society.
- [22] C. Ataca, H. Şahin, and S. Ciraci, “Stable, Single-Layer MX_2 Transition-Metal Oxides and Dichalcogenides in a Honeycomb-Like Structure,” *The Journal of Physical Chemistry C*, vol. 116, pp. 8983–8999, Apr. 2012. Publisher: American Chemical Society.
- [23] H. Haug and S. W. Koch, *Quantum Theory Of The Optical And Electronic Properties Of Semiconductors (5th Edition)*. World Scientific Publishing Company, Jan. 2009. Google-Books-ID: 1J1IDQAAQBAJ.
- [24] C. Zhang, A. Johnson, C.-L. Hsu, L.-J. Li, and C.-K. Shih, “Direct Imaging of Band Profile in Single Layer MoS_2 on Graphite: Quasiparticle Energy Gap, Metallic Edge States, and Edge Band Bending,” *Nano Letters*, vol. 14, pp. 2443–2447, May 2014. Publisher: American Chemical Society.
- [25] D. Erben, A. Steinhoff, C. Gies, G. Schönhoff, T. O. Wehling, and F. Jahnke, “Excitation-induced transition to indirect band gaps in atomically thin transition-metal dichalcogenide semiconductors,” *Physical Review B*, vol. 98, p. 035434, July 2018.
- [26] D. Erben, A. Steinhoff, M. Lorke, and F. Jahnke, “Optical nonlinearities in the excited carrier density of atomically thin transition metal dichalcogenides,” *Physical Review B*, vol. 106, p. 045409, July 2022.
- [27] C. D. P. Vo and T. D. Huynh, “Calculation of shift current tensors in two-dimensional transition metal dichalcogenides,” *E3S Web of Conferences*, vol. 496, p. 02002, 2024. Publisher: EDP Sciences.